Small transcriptional differences lead to distinct NF-κB dynamics in quasi-identical cells

Cise Kizilirmak[1,2], Emanuele Monteleone[1,2], José Manuel García-Manteiga[3], Francesca Brambilla[2], Alessandra Agresti[1,2], Marco E. Bianchi[1,2,*] and Samuel Zambrano [1,2,4,*]

[1]School of Medicine, Vita-Salute San Raffaele University, Milan, 20132, Italy.

[2] Division of Genetics and Cell Biology, IRCCS San Raffaele Scientific Institute, Milan, 20132, Italy.

[3] Center for Omics Sciences. IRCCS San Raffaele Scientific Institute, Milan, 20132, Italy.

[4] Lead contact.

[*] Correspondence to : M.E.B: bianchi.marco@hsr.it SZ: zambrano.samuel@hsr.it.

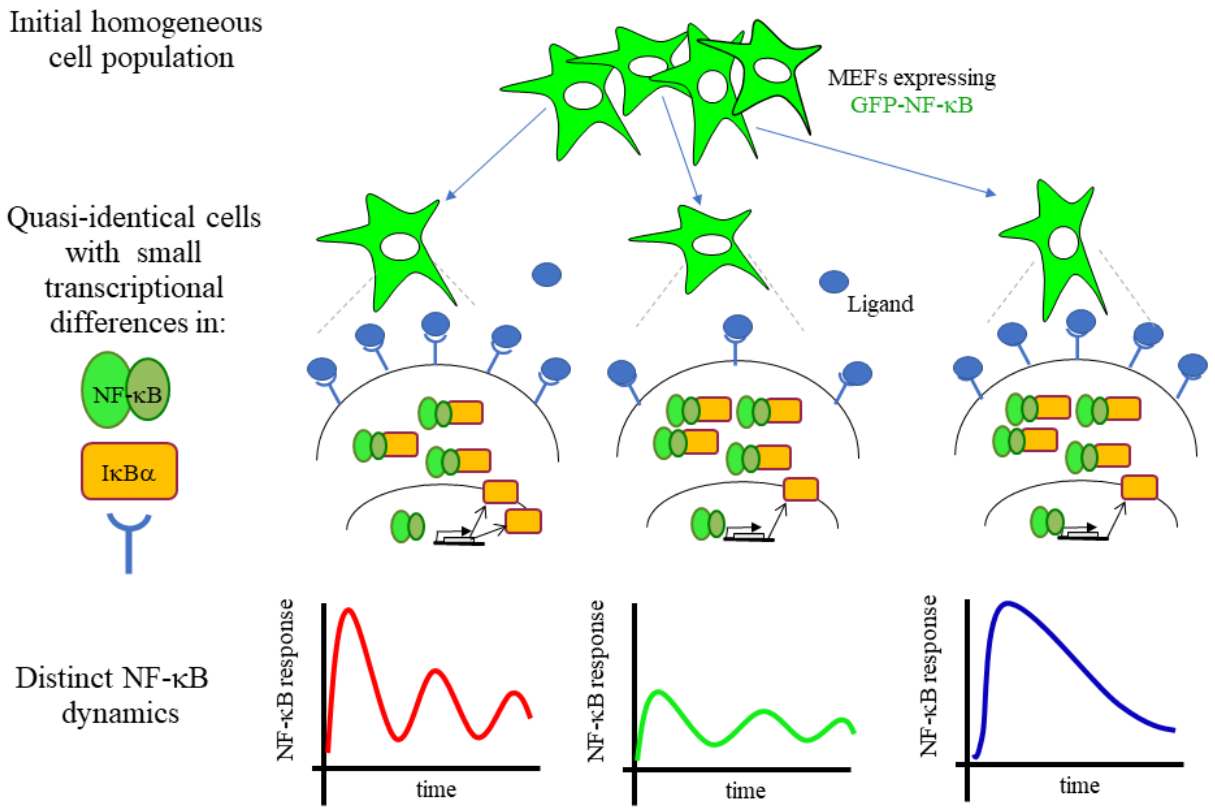

ABSTRACT

Transcription factor dynamics is fundamental to determine the activation of accurate transcriptional programs and yet is heterogeneous at single-cell level, even between very similar cells. We asked how such heterogeneity emerges for the nuclear factor κB (NF-κB), whose dynamics have been reported to cover a wide spectrum of behaviors, including persistent, oscillatory and weak activation. We found that clonal populations of immortalized fibroblasts derived from a single mouse embryo (that can hence be considered quasi-identical) display robustly distinct dynamics upon tumor necrosis α (TNF-α) stimulation, which give rise to differences in the transcription of NF-κB targets. Notably, standard transcriptomic analyses indicate that the clones differ mostly in transcriptional programs related with development, but not in TNF-α signaling. However, by combining transcriptomics data and simulations we show how the expression levels of genes coding for proteins of the signaling cascade determine the differences in early NF-κB activation; differences in the expression of IκBα determine differences in its persistence and oscillatory behavior. The same analysis predicts inter-clonal differences in the NF-κB response to IL-1β. We propose that small (less than twofold) differences at transcript level are a source of heterogeneity in TF dynamics within homogeneous cell populations, and all the more so among different cell types.

INTRODUCTION

Cells are able to provide precise transcriptionally-mediated responses to the complex mixture of external and internal stimuli to which they are subjected (Milo and Phillips, 2015). In this context, a key role is played by transcription factors (TFs), proteins that are "activated" upon stimuli and selectively trigger the expression of target genes coding for proteins required for an adequate response. The activation of several TFs is primarily mediated by their nuclear accumulation and is tightly regulated by other players within their genetic regulatory circuit, whose design contributes to providing a specific transcriptional output given a certain input (Alon, 2007). The nuclear accumulation of TFs is dynamic and can be oscillatory, as shown first for circadian rhythms in response to the day/night cycle (Patke et al., 2020) and the cell cycle (Ferrell et al., 2011); oscillations were then discovered for a wide variety of TFs (Levine et al., 2013). The emerging view is that such dynamics is not merely a by-product of the regulatory mechanisms of the TFs, but that it has a functional role in gene expression (Purvis and Lahav, 2013) and impacts a wide array of cellular process, e.g. determining cell fate (as for p53, (Purvis et al., 2012)), the response to mechanical cues (as for YAP/TAZ, (Franklin et al., 2020)) or the speed of the segmentation clock during embryo development (as for Hes7, (Matsuda et al., 2020)). Of note, single cell measures show consistently a high degree of heterogeneity in TF dynamics within a population, which yet is compatible with the TFs' ability to provide an accurate transcriptional output given an input (Selimkhanov et al., 2014).

The NF-κB system is a paradigmatic example of the dynamic nature of TF activation (Kizilirmak et al., 2022). NF-κB is a family of dimeric TFs that plays a central role in innate and adaptive immune responses (Hayden and Ghosh, 2008; Natoli and Ostuni, 2019); dimers including the monomer p65 have the strongest transcription activating potential (Schmitz and Baeuerle, 1991) and are involved in the canonical pathway (we'll refer to such dimers as NF-κB in what follows). NF-κB is kept in the cytosol bound by its inhibitors IκB, which are degraded upon external inflammatory stimuli such as the cytokine Tumor Necrosis Factor alpha (TNF-α) and are themselves NF-κB transcriptional targets (Hoffmann et al., 2002). It was immediately evident that this system of negative feedbacks could lead to oscillations in the nuclear concentration of NF-κB upon stimulation, as confirmed by an ever-growing list of live cell imaging studies (Nelson et al., 2004; Sung et al., 2009; Tay et al., 2010; Zambrano et al., 2014a). NF-κB nuclear localization dynamics (in short, NF-κB dynamics) have the potential to discriminate between ligand dose (Zhang et al., 2017) and type (Adelaja et al., 2021; Martin et al., 2020) and determines target gene expression (Ashall et al., 2009; Lee et al., 2014; Sung et al., 2009; Tay et al., 2010) in a functionally relevant way (Zambrano et al., 2016). However, terming such dynamics "oscillatory" is somewhat simplistic: the dynamics can be qualitatively quite different between cell types, ranging from sustained oscillations with a period of 1.5 hours for 3T3 cells (Kellogg and Tay, 2015), damped oscillations for mouse embryonic fibroblasts (Zambrano et al., 2016), persistent nuclear localization for RAW or 3T3 cells upon LPS (Lee et al., 2009; Sung et al., 2014) and non-oscillatory for HeLa cells (Lee et al., 2014). Even within a population of cells of the same type, individual cells display dynamical heterogeneity and qualitatively different dynamics, with cells that oscillate and cells that do not (Nelson et al., 2004; Zambrano et al., 2014a). How different NF-κB dynamics arise, in particular within fairly homogeneous populations, is far from being clear and yet distinct dynamics are crucial for cell specificity and can have

important functional consequences, for example in the cell's life-death decisions (Lee et al., 2016), its epigenetic state (Cheng et al., 2021) and even for the cell's commitment to differentiation (Kull et al., 2022). Understanding how different dynamics emerge can shed light on how the NF-κB system uses dynamics in a cell-specific way to produce a desired output given a certain input, and more in general on the mechanisms by which cells within a population produce distinct TF dynamic responses to stimuli.

Here, we focused on immortalized GFP-NF-κB mouse fibroblasts (MEFs) derived from a single embryo. Yet, in these cells qualitatively and quantitatively different dynamics can be observed (De Lorenzi et al., 2009; Sung et al., 2009; Zambrano et al., 2014a, 2016). To determine the molecular mechanisms responsible for such dynamical variations, we isolated several clones from the original cell population. Cells within each clone are genetically and epigenetically identical, and cells from different clones can be considered "quasi-identical": they share the same genome derived from a single individual, albeit with sparse genetic variations accumulated during in vitro cultivation and immortalization, while their epigenetics reflects their heterogeneity in identity according to anatomical site of origin (Lynch and Watt, 2018) . We found that each clonal population has a distinct and heritable NF-κB dynamics upon TNF-α. We focused on three archetypical clones with persistent, oscillatory and weak responses, that we show correlate with the transcription levels of NF-κB target genes. We develop a framework for transcriptomic-constrained numerical estimation of the number of NF-κB activating complexes formed upon TNF-α or IL-1β, and we show that it is predictive of the relative strength of the early response to both inflammatory stimuli. Differences in expression of genes in the NF-κB signal transduction pathway, combined with small but robust transcriptional differences in the expression of the key negative feedback IκBα, explain the differences in the persistence of NF-κB activation in the clones. Indeed, we show how interfering with the expression of the repressor IκBα can make cells switch from a sharp response to a more persistent nuclear localization dynamics, as predicted by our mathematical model.

Taken together, our results show that small differences in the expression levels of the genes of the NF-κB signaling pathway can produce distinct responses in cells of the same type derived from the same organism, that we refer to as quasi-identical. This mechanism explains how multicellular organisms can produce diverse cell types with selective and specialized NF-κB-mediated response to inflammatory stimuli.

RESULTS

1. Clonal populations of fibroblasts derived from a single embryo display distinct NF-κB dynamics upon TNF-α

Different NF-κB dynamics have been reported in different cell types, so here we decided to focus on dynamics of quasi-identical cells: immortalized mouse embryonic fibroblasts (MEFs) derived from a single mouse homozygous GFP-p65 knock-in embryo ((De Lorenzi et al., 2009) and **Methods**). We stimulated our GFP-p65 MEF population with 10 ng/ml tumor necrosis factor alpha (TNF-α) and quantified the nuclear to cytosolic intensity (NCI) of NF-κB using our established method of live cell imaging (Zambrano et al., 2014a, 2016), and **Methods**). As previously reported (De Lorenzi et al., 2009; Sung et al., 2009; Zambrano et al., 2014a, 2016) the response of these MEFs upon TNF-α is heterogeneous (**Figure 1A** and **Movie S1**). Most cells display oscillatory peaks of nuclear localization while others display a non-oscillatory dynamics (**Figure 1B**), a kind of dynamics also referred to as "persistent activation" and similar to the one reported for macrophages (Cheng et al., 2021; Sung et al., 2014) and fibroblasts (Lee et al., 2009) upon lipopolysaccharide (LPS) stimulation. We can indeed analyze NF-κB dynamics of hundreds of cells (see **Methods** and **Figure S1A**) and plot them to form a "dynamic heatmap" which captures the dynamics across the cell population (**Figure 1C**).

Starting from our original population of MEFs (that we refer to as the "pool" in what follows) we generated 17 clonal populations following standard procedures (**Figure 1D** and **Methods**). Eight clonal populations were imaged upon stimulation with 10 ng/ml TNF-α. Of note, these populations cannot be properly referred to as sub-clonal since the original population (the pool) does not derive from a single clone; instead, the pool is the result of a number of passages from a population of primary MEFs (see **Methods**), analogously to the procedure used to generate 3T3 cells (Amand et al., 2016; Gapuzan et al., 2005). We expect a small degree of genetic heterogeneity due to somatic mutations (Milholland et al., 2017) in the embryo and in the replications during the passages (we address this in further detail below). We found that NF-κB dynamics of each clonal population upon TNF-α was markedly different, even if a certain degree of intra-clonal heterogeneity was observed (**Figure 1E**). To have an unbiased confirmation of this observation, we utilized an unsupervised stochastic clustering approach (see **Methods**), which grouped NF-κB dynamic profiles of the clones and the pool according to their shapes into 9 different clusters (**Figure S1B**). For each realization of the clustering, we obtain a histogram with the number of profiles of a given population falling in each cluster (**Figure S1C**), that can be plotted together in a colormap (**Figure S1D**). Both single realizations of this procedure (**Figure S1D**) and the average of many (**Figure 1F**) indicate that NF-κB dynamic profiles of cells of the same population are more likely to cluster together than with profiles of cells of other populations (elements in the diagonal have higher values). Interestingly, this is less evident for cells from the pool, which tend to be more evenly distributed across the clusters where some of the clones are the majority (see arrow, **Figure 1F**), indicating that the dynamics of each clonal population mirror that of certain subpopulations within the pool. An entropy-based clustering disorder degree parameter (see **Methods**) based on these probabilities gives significantly lower values when the profiles are assigned to the proper clonal population (they are more

"ordered" by the clustering) than when they are randomly mixed and then stochastically clustered (**Figure 1G**), further indicating that NF-κB profiles within a clonal population are similar.

In sum, we can isolate clones from a population of MEFs derived from a single embryo that have distinct dynamical behaviors, which mirror those of individual cells in the original cell population.

2. NF-κB dynamics and oscillatory behavior are clone-specific and yet heterogeneous within clonal populations

We then chose 3 clones with archetypical dynamics reminiscent of those observed in the literature and in cells in our original MEF population (**Figure 1B**): a clone with more persistent nuclear localization of NF-κB (clone B, blue), one more oscillatory with a first well-defined sharp peak (clone R, red) (in other words, a nuclear localization that decreases fast (Zambrano et al., 2020) and a clone characterized by a low activation of NF-κB (clone G, green) (**Figure 1E**).

Clonal populations R, G, and B showed clearly distinct NF-κB dynamics even by direct inspection of their timelapses (**Figure 2A** and **Movie S2-S4**). The average NF-κB activation profiles (**Figure 2B**) show that clone B gets more activated than clone R, and clone R than clone G: we can say they follow the order relation B>R>G. Such differences were strikingly robust across replicated experiments (examples of replicates shown in **Figure S2A**) and were conserved also for higher TNF-α doses (100 ng/ml) (**Figure S2B**). Importantly, these differences were also conserved after many cell divisions and culture passages, even if the average response to TNF-α was weaker for all clones after 8 weeks in culture (**Figure S2C**).

We then investigated the dynamics of each clone at single-cell level. The dynamic variability calculated through the coefficient of variation showed that clones' dynamics have slightly less variability than the pool (**Figure S2D**). Next, we focused on typical single cell quantifiers of NF-κB dynamic response, such as the early NF-κB response of each cell (value of the first peak), its timing and the area under the curve (Tay et al., 2010; Zambrano et al., 2014). We found that the values of such quantifiers are heterogeneous among cells of the same clone, although the differences are statistically significant between the clones and remarkably similar across replicates (**Figure 2C** and **Figure S2E**). The NF-κB response is typically higher for cells of clone B than for cells of clone R, which in turn have much higher peaks than cells of clone G (**Figure 2C**), so the B>R>G relation is preserved at single-cell level. Interestingly, clone G has the lower peak value in spite of having the higher basal levels of nuclear NF-κB (**Figure S2F**), resulting in an even lower fold change of nuclear NF-κB upon TNF-α with respect to the other clones (a key factor for gene expression (Lee et al., 2014)), is also different across the clonal populations. The timing of the NF-κB response is equally prompt within our experimental resolution in clones B and R, but slightly slower in clone G (**Figure 2C**). The larger differences though are observed in the area under the curve (**Figure 2C**), which is much bigger for clone B than for clone R, and is again the smallest for clone G. This captures well our observation that clone B has a more persistent NF-κB nuclear localization dynamics, while clone R displays a sharper response. We did also verify that all the differences above hold true

when considering the absolute intensity of the nuclear signal (**Figure S2G**) instead of the nuclear to cytosolic intensity of NF-κB, and also when we manually segmented the cells' nuclei (**Figure S2H**).

The differences between clonal populations could be related to factors such as cell cycle, which has been already shown to modulate the response to TNF-α (Ankers et al., 2016). Thus, we compared the cell cycle distributions of our populations (see **Methods**, **Figure S2I** and **Table 1**). Clone B and Clone G have very similar distributions, but they display the clearest differences in the dynamics of NF-κB response, suggesting that the cell cycle has a limited impact on their inter-clonal dynamic differences. Clones B and R are more different, so we applied a computational correction for the differences in the population fractions in each cell cycle phase (assuming that the stronger response in clone B is due to a higher fraction of cells in phase S than in clone R and correcting for this, details in **Methods**); even so, the differences were maintained (**Figure S2J**).

Our single cell data does also provide us an interesting perspective on whether NF-κB signaling dynamics can be considered oscillating or not, a topic that has been subjected to discussion (Barken et al., 2005; Kellogg and Tay, 2015; Nelson et al., 2004; Zambrano et al., 2016). Oscillations are characterized by the presence of multiple peaks in the NF-κB dynamic profiles. We calculated the fraction of cells with 1, 2 or 3 oscillatory peaks within each clonal population upon treatment with 10 ng/ml for 4 hours (**Figure 2D**) or longer (**Figure S2K**). We find that each clone contains a different fraction of cells that do not oscillate; however, there are also cell fractions in each clonal population that have two or more peaks and can be considered "oscillatory". Examples of each type of dynamics for each population are shown in **Figure 2D**. The period of the oscillations, computed as inter-peak timing, is heterogenous but slightly higher for clone B (**Figure 2E**). Consistently with the dynamic heterogeneity found in each cell population, we find variability in the peak value ratios (**Figure 2F**) which is again maintained in experimental replicates (**Figure S2L**). Our data then show that being "oscillatory" is somehow a "fuzzy" phenotype and even clones derived from a population of quasi-identical cells can be considered oscillatory to different degrees. This compares with the qualitatively different dynamics observed for different cell types, that can go from cells that can oscillate in a sustained fashion for 20 hours and more (Kellogg and Tay, 2015) to those that oscillate in a more damped way with fewer oscillatory peaks (Zambrano et al., 2016) or do not oscillate at all (Lee et al., 2014); our experiments demonstrate that heterogeneous dynamics can be found even within very homogeneous populations, as our clones.

Overall, our data shows how clonal populations of quasi-identical MEFs derived from the same mouse embryo have distinct dynamical features at population level both in their early response to TNF-α and in the subsequent dynamics, which is oscillatory to a different degree within each population. Yet, the dynamics is still considerably heterogeneous at single-cell level within each clonal population.

3. Clonal populations have distinct transcriptional programs and control of target gene expression upon TNF-α

To further investigate to what extent our clonal populations are different and to gain insights on how NF-κB controls target gene expression in each of them, we next performed RNA-sequencing. Our clones display quantitative differences in their average NF-κB dynamic response already after 1 hour TNF-α stimulation (**Figure 2B**). Therefore, we performed RNA-sequencing after 1 hour (**Figure 3A**). To gain statistical power, we generated 5 replicates per condition (see **Methods**). All replicates were of good quality with more than 10000 genes with CPM>1 (see **Methods** and **Figure S3A**). RNA sequencing already provides insight on the genetic homogeneity of the populations: these cells were immortalized following the 3T3 procedure from primary MEFs of the same embryo, a procedure that requires 20-30 passages (see **Methods**). Indeed, using an established reads mapping procedure (see **Methods**) we confirmed a frequency of single base substitution among clones (**Figure S3B**) compatible with the somatic mutation frequency found in cells of the same mouse (Milholland et al., 2017), as expected for cells derived from the same embryo and subject to a low number of passages.

We then performed a PCA of our samples' transcriptomes (see **Methods**) and found that samples from different clones do cluster in different groups (**Figure 3B**). Such neat clustering is also preserved in additional dimensions and few dimensions are required to explain most of the variability (**Figure S3C**). Of note, the apparent transcriptional divergence between our clones is small: when we performed our PCA including also public transcriptomic data from other tissues (see **Methods**), the samples from our populations cluster very closely together and far from the outgroup sample (**Figure S3D**). To get an unbiased insight on potential biological differences between our cell populations, we then looked at genes differentially expressed between clones that were untreated, which are in principle the most informative from the point of view of the cell's identity. The categories enriched (see **Methods**) are mostly related to morphogenesis of different organs/tissues: epithelium, renal system and skeletal system, to cite a few (**Figure 3C**). This suggests that our clonal MEF populations conserve characteristics of the primary MEFs that were presumably already committed to different tissues or anatomical compartments, as expected (Lynch and Watt, 2018). The only categories reminiscent of NF-κB activation are "immune response-regulating signaling pathway", "immune response-regulating cell surface receptor pathway", "negative/positive regulation of response to external stimulus" and "regulation of leukocyte activation" (**Figure 3C**). The *wikipathways* database provides a list of hundreds of genes (see **Methods**) involved in TNF-α signaling. Of note, mutation calling did not highlight any differences in the mRNA sequences of these genes (see **Methods**). Such genes cluster nicely by clones and treatments and seem more highly expressed in clone G for most of the genes (**Figure S3E**), so this classical unbiased analysis does not provide predictive insights on why the clones respond with different strength to TNF-α.

We next decided to focus on how NF-κB controls gene expression. First, we focused on 462 genes that we previously established as differentially expressed upon TNF-α stimulation (Zambrano et al., 2016). Interestingly, using this gene set the PCA now clusters samples both by treatment and by clone (see **Figure 3D** and **Methods**). This also applies when considering additional PCA dimensions, while again few

dimensions are required to explain the global transcriptomic variability for this specific gene set (**Figure S3F**). We then had a closer look to the genes differentially expressed upon TNF-α for each clone (see **Figure 3E**, **Figure S3G** and **Methods**). Interestingly, the number of up-regulated genes correlates well with the strength of the NF-κB response and satisfies the same order relation B>R>G (**Figure 3E**), and the fold change of the genes differentially up-regulated also follow on average the B>R>G relation (**Figure 3F**). When performing gene set enrichment of up-regulated genes, the recurrent categories include TNF-α signaling pathway and innate immune responses as expected (see **Methods** and **Figure S3H**), but with different degrees of overlap with the different categories, suggesting that the clones activate slightly different transcriptional programs upon TNF-α.

Our data show that the clones differ mostly for developmental identity and suggest that clonal differences in the strength of the NF-κB response are a key determinant of the expression level of NF-κB target genes upon TNF-α exposure. Clones differ transcriptionally mostly in GO terms not related to NF-κB, although genes belonging to the TNF-α signaling circuitry are also differentially expressed across the clones. However, this provides limited insight as to why the early NF-κB response follows the B>R>G order relation and on the differences in the dynamics. Hence, we tried to gain additional mechanistic insight from our transcriptomic data by focusing on key players of NF-κB activation and describing mathematically the activation process.

4. Transcriptomic-constrained estimations of differences in the number of activating complexes between the clones explains the differences in their NF-κB responses

The activation of NF-κB upon TNF-α follows the interaction of the ligand with its receptor, which leads to the formation of the so-called Complex I by the sequential association of different proteins: an "activating complex" (DeFelice et al., 2019; Hayden and Ghosh, 2008; Hsu et al., 1996; Lee et al., 2016; Wilson et al., 2009). Activating complexes recruit and activate the IKK complexes (**Figure 4A**), which in turn determine the nuclear translocation of NF-κB (Cruz et al., 2021). We then reasoned that transcriptomic data might provide insights on whether different numbers of activating complexes are formed in the clones upon stimuli, resulting in the different NF-κB early responses observed (the first peak). We assumed that the level of RNA expression of the genes involved in the formation of the activating complex in untreated cells (since NF-κB response takes 30 minutes, hence is too fast to be impacted by TNF-α induced transcriptional effect) is proportional to their protein amount in the three clones; this is for example the case for p65 (**Figure S4A**). We elaborated the list "TNF-α to NF-κB" of genes coding for proteins forming the activating complex based on the existing literature (DeFelice et al., 2019; Hayden and Ghosh, 2008; Hsu et al., 1996; Lee et al., 2016; Wilson et al., 2009) (see **Figure 4A** and gene list in **Methods**) and found that the variation in their expression is quite small, less than 50% with respect to clone R (**Figure S4B**). Furthermore, single sample Gene Set Enrichment Analysis (Barbie et al., 2009) was performed for each of three clones to elucidate the enrichment of "TNF-α to NF-κB" list when compared to each other and to the original cell pool, but we did not find statistically significant

differences (see **Methods** and **Figure S4C**). Taken together, our bioinformatic analysis of the "TNF-α to NF-κB" list cannot explain the differences in the NF-κB responses observed between the clones.

We then moved to a more detailed description of the events leading to NF-κB activation. Activating complex formation can be considered as a sequential series of association (and dissociation) reactions of the proteins coded by genes of the "TNF-α to NF-κB" list, each with their characteristic dissociation constants K_D that we assume to be reached fast upon stimulus (see **Methods**). The total abundance of the complex will then be limited by the less abundant component (it is not possible to have more copies of the complex $(A{:}\,B)$ than the minimum of A and B abundances, see **Methods** and **Figure S4D**). In our "TNF-α to NF-κB" list, the less abundant protein is known to be the receptor TNFR1 (encoded by *Tnfrsf1a*) of which there are about 10^3 copies, while the abundance of downstream proteins is about 10^6 (Cruz et al., 2021; Hwang et al., 2015). Hence TNFR1 is the limiting factor in the formation of activating complexes formed and the number of such complexes will be largely determined by its abundance (see **Methods**), irrespectively of the relative abundances of other proteins that are three orders of magnitude more abundant than TNFR1. Interestingly, transcriptomic data shows that the expression of TNFR1 in untreated samples follows the order relation of B>R>G (**Figure 4B**) which in principle leads to a number of activating complexes following B>R>G, which correlates with the experimentally observed ranking in the early NF-κB response upon TNF-α.

To further test whether the order relation B>R>G would also hold when the processes of association-dissociation involved in complex formation and all the relative abundances are considered in detail, we devised a transcriptomic-constrained numerical approach to estimate the fold change (FC) differences in number of complexes between the clones (**Figure 4C**). We simulate the association reactions between the elements of the "TNF-α to NF-κB" list leading to the formation of the activating complex, each characterized by their dissociation constant K_D, which we consider equal for all the clones for each reaction (see **Methods**). In such simulations we assume that the FC in protein abundances between clones matches the FC of transcript abundances, as for p65 (**Figure S4A**). The average protein abundance of each element in the list across clones is chosen randomly in each numerical simulation, but taking into account the difference in orders of magnitude between the abundance of the receptor ($O(10^3)$) and the remaining proteins ($O(10^6)$), that is Δ=3 (Cruz et al., 2021; Hwang et al., 2015). Numerical estimates (**Figure 4D**) predict an order relation B>R>G for a wide range of order of magnitudes of the K_D values, although variability increases for high K_D, a situation where the number of complexes resulting is low (see **Figure S4D** and **Methods**). We also evaluated the dependence of the result in Δ by performing simulations in the limit situation K_D =0, where the association between the proteins that form the complex is perfect, and for Δ values much lower than the experimentally observed ones: we find that the transcriptomic- constrained predictions of the number of complexes converge quickly to a B>R>G ranking (**Figure 4E**). Simulations in the K_D-Δ parameter space confirm these trends (**Figure S4E** and **S4F**) and show that the order relation of the number of activating complexes B>R>G holds for a wide parameter range.

To test whether the predicted small differences in the number of activating complexes can explain the different responses observed we developed a simple mathematical model of NF-κB signaling based on

previous ones (Zambrano et al., 2014b, 2016) (see **Methods** and **Figure 4F**). In our model, the number of activating complexes determines the activation of the IKK kinases, so the NF-κB response and complex numbers correlate (Cruz et al., 2021) (**Figure 4G**). We can then use this model and fit the FC in the number of complexes of B vs R and G vs R taking also into account the variations in NF-κB amount across clones (**Figure S4A**), which alone has a small impact (**Figure S4G**); a result is shown for a given parameter set (provided in **Table 3**) in **Figure S4H**. We repeated this fitting for different randomizations of the initial parameters of the model to find the combinations leading to changes in the early NF-κB response of clones B and G with respect to R as those experimentally observed upon TNF-α (see **Methods** and examples in **Figure S4I**). The results (**Figure 4H**) indeed show that for most parameter sets small changes in the number of activating complexes are enough to fit the differences in the early response observed, with values within the range of those obtained from our transcriptome-constrained estimations (compare **Figure 4D, 4E** with **Figure 4H**).

Taken together, our numerical approach suggests that small differences in the transcription levels of the TNF-α receptor are responsible for the differences in the early NF-κB responses observed between the clones. Transcriptomic-constrained estimations show that the relation B>R>G in the number of activating complexes would hold for a large range of values of the parameters involved and would lead to differences that are enough to explain the differences in the NF-κB response between the clones.

5. Transcriptomic-constrained simulations predict differences in early NF-κB activation between the clones upon IL-1β

Since our transcriptome-constrained estimations are predictive of the differences in the early response between the clones to TNF-α, we asked if they could also predict the differences in the response to a different inflammatory stimulus. We focused on IL-1β, a cytokine that is known to activate NF-κB through a pathway only partially overlapping with that of TNF-α, and characterized by its own regulatory mechanisms and dynamical features (DeFelice et al., 2019; Martin et al., 2020). We elaborated a list of "IL-1β to NF-κB" genes coding for proteins that are involved in the formation of the activating complex arising upon interaction of IL-1β with its receptor (Martin and Wesche, 2002) (elements shown in **Figure 5A,** gene list in **Methods**). The list now includes genes coding for the subunits of the dimeric receptor, *Ilr1r1* (coding for IL-1R1) and *Il1rap* (coding for IL-1R3). In this list, differences in expression typically do not exceed 2-fold (**Figure S5A**), ssGSEA finds a difference between clone B and the other samples, but not between the remaining ones (**Figure S5B**). For this signaling system the limiting factor is the abundance of IL-1R3, of which there are $O(10^2)$ copies, one order of magnitude less than for IL-1R1, and $\Delta \gtrsim 3$ orders of magnitude less abundant than the remaining downstream proteins (Cruz et al., 2021; Hwang et al., 2015). Interestingly, we found the expression of *Il1rap* in the untreated samples follows the order relation B$\gtrsim$G>R, since the differences between B and G are not significant but for both it is more highly expressed than for R (**Figure 5B**). Thus, the expectation is that the number of activating complexes formed by the clones should follow the order B$\gtrsim$G>R.

We then performed our transcriptomic-constrained estimation of the FC variation in the number of activating complexes between clones for a wide variety of conditions (see **Methods**). Given Δ=3 we find that the relation B>G>R holds for a wide range of values of K_D (**Figure 5C**) but with a higher variability than for TNF-α, in particular for high K_D, so B≳G>R would be more accurate. We also find that the estimations quickly converge to B≳G>R for Δ values smaller than the one experimentally verified (**Figure 5D**). These trends are also confirmed when we analyze the K_D-Δ parameter space (**Figure S5C** and **S5D**). Following the procedure described for TNF-α, we fitted our mathematical model of NF-κB dynamics to find what FC variation of the number of activating complexes could reproduce the observed differences in the response (example for one parameter set shown in **Figure S4H**), and we obtained values within the range predicted by our transcriptomic-constrained estimation approach (**Figure 5E**). Overall, this analysis suggests that the number of activating complex upon IL-1β shall follow the relation B≳G>R, with B and G having similar NF-κB responses and both with a response stronger than R.

To test this prediction, we performed live cell imaging of the clones upon 100 ng/ml IL-1β. All clones respond, and in particular now clone G has a stronger response to IL-1β than to TNF-α with a similar early NF-κB response (first peak value) to that of clone B (**Movies S5 and S6** and **Figure 5F**); notably, the average NF-κB response reflects the order relation B>G>R with clone B and G having similar first peak value (**Figure 5G**), as predicted. We found these differences are also clear when considering single-cell data (**Figure 5H, S5E**), where clone G cells display overall a stronger response than clone R cells. However, clone B is the one with a higher response and a much higher AUC. Finally, upon IL-1β we find that the cells' oscillatory phenotype is also heterogeneous for each clone (**Figure 5I**), but different relative to TNF-α: more cells of clone G have at least two peaks (**Figure 5I**) and an oscillatory period at T=1.5h, similar to clone R (**Figure 5J**). Clone B remains the one with a less oscillatory phenotype (**Figure 5I**), suggesting that this behavior might be related with downstream regulators of NF-κB activity, an idea that we explore next. As with TNF-α, the parameters describing the oscillations are also heterogeneous across the clones (**Figure S5F**).

Taken together, our transcriptome-constrained estimation approach predicts that a small difference in the expression of the protein that is the limiting factor for formation of the activating complex upon IL-1β (the IL-1R3 receptor subunit) would lead to the B≳G>R ranking, a prediction that is confirmed by live cell imaging experiments.

6. Differences in the expression levels of the negative feedbacks underpin distinct NF-κB dynamics in quasi-identical cells

Beyond differences in the peak of the response, our clonal populations also show differences at later time points. For the sake of simplicity we focus on the case of clone B having a more persistent NF-κB response as compared to clone R to TNF-α, which is translated into higher AUCs for NF-κB dynamic profiles (**Figure 2C**): robust B>R relations are observed for both stimuli. This is also the case upon IL-1β (**Figure 5H**). We performed numerical simulations showing that by changing the NF-κB amount and the number of activating complexes to match the differences in the early responses, only minor changes in the AUC are obtained (example shown in **Figure S6A**), well below the experimental differences observed between clone B and R (**Figure 6A**).

To explain these differences in AUCs, we then decided to focus on the negative feedback. Our transcriptome data indeed show that the expression of IκBα upon 1 h TNF-α (when it peaks) follows a R>B>G pattern (**Figure 6B**) confirmed by RT-qPCR (**Figure S6B**); the remaining negative feedbacks of the system (Ashall et al., 2009; Hoffmann et al., 2002) have a moderate effect in the short-term dynamic response (Paszek et al., 2010; Son et al., 2021) and are comparatively expressed at much lower levels (**Figure S6C**). To dissect the contribution of each of the experimentally observed differences in the dynamics, we performed experimentally constrained numerical simulations of our mathematical model with randomized parameters for clone R, where we sequentially adjust the amount of NF-κB, together with the number of activating complexes to match the experimentally observed response, and the transcription rate of *Nfkbia* transcription rate so it fits the experimentally observed differences in the expression level of B respect to R. (**Figure 6C** and **6D** and **Methods**). Of note, only the latter combination of changes results in a change in the AUC even bigger than the difference observed between clone B and clone R, in stark contrast with the effect of the other changes, even combined (**Figure 6E**). Furthermore, when we analyze the effect of each correction on the oscillatory profiles of our randomizations of the parameters of R, we find that the modulation of *Nfkbia* is determinant in producing less oscillatory profiles (**Figure 6F**), something that can also be observed in the examples displayed in **Figure 6D**. This indicates that the experimentally constrained small differences in these model parameters, combined, are sufficient to explain why clone B and R display a persistent and a sharp response, respectively, and why clone R has more oscillatory dynamics than clone B.

We set out to experimentally test the effect of modulating IκBα levels in the dynamic response to TNF-α. To modulate the IκBα mRNA levels we took advantage of antisense oligonucleotide (ASO) technology (see **Methods**). The single-stranded synthetic 2'-deoxy-2'-fluoro-β-d-arabino nucleic acid (FANA) oligos were designed to be self-delivered to the cells and to be fully complementary to IκBα mRNA, inducing mRNA cleavage by RNAseH and reducing the synthesis of the IκBα protein (see **Methods**). We pre-treated for 24 hours clones R and B with different concentrations of the ASO, whose internalization was visible (**Figure S6D**), and this led to a moderate but significant decrease on the mRNA levels of IκBα (**Figure S6E**). We indeed observed that, upon TNF-α, the response of both clone B and clone R was characterized by more persistent NF-κB nuclear localization, indicating that partial transcriptional

disruption of the IκBα negative feedback is enough to produce a qualitative change in the dynamics (**Figure 6G**). This was also the case when pre-treating with ASOs our MEFs pool (**Figure S6F**, **Movies S7** and **S8**). A more detailed quantification of the dynamics shows that the maximum value of the NF-κB response increases slightly in ASO-treated cells in clone R (**Figure 6H**). However, the area under the curve upon TNF-α increases for both clones, and in particular for clone R, so that the AUC of ASO-treated clone R is much more similar to that of clone B (**Figure 6I**). This trend is reproducible in replicates (**Figures S6G, S6H**). The effect of the ASOs in clone R can be reproduced in numerical simulations with our models where we only adjust *Nfkbia* expression levels following the experiments (see **Figure 6J** and **Methods**).

Overall, we have predicted through mathematical modeling that small changes between clone B and clone R in the expression levels of the negative feedback can shift the dynamics from a sharp versus a persistent NF-κB response. Our experiments with ASOs show how even a mild targeted modulation of the expression of IκBα can alter the dynamics of clone R to resemble that of clone B, and therefore to reprogram it from a sharp (and oscillatory) NF-κB activation to a persistent response, as predicted by our mathematical models.

DISCUSSION

A population of MEFs with heterogeneous NF-κB dynamics is composed by quasi-identical cells with distinct dynamics. Single-cell imaging studies of NF-κB dynamics have shown that there is a high degree of heterogeneity within homogeneous cell populations (Lee et al., 2014; Nelson et al., 2004; Paszek et al., 2010; Sung et al., 2009; Tay et al., 2010; Zhang et al., 2017). Our work, performed on a cell population of fibroblasts derived from a single mouse embryo and immortalized by serial passages indicates that NF-κB dynamic heterogeneity might be due in part to the coexistence of quasi-identical cells that do respond distinctly to the stimuli. Extrinsic factors such as the cell cycle phase have been shown to affect NF-κB dynamics (Ankers et al., 2016) but we cannot attribute inter-clonal differences to differences in the cell cycle. Instead, we show here that the expression levels of genes coding for key elements of the NF-κB signaling pathway can explain the clonal differences.

Transcriptomics is predictive of the clonal response to stimuli. The link between NF-κB dynamics and transcription is typically analyzed in one direction: how does NF-κB nuclear localization dynamics drive gene expression? (Lane et al., 2017; Lee et al., 2014; Sen et al., 2020; Tay et al., 2010; Zambrano et al., 2016). Here we consider the same question in the other direction: how can transcriptomic differences affect dynamics? We developed a computational framework based on transcriptomic-constrained estimation of the number of activating complexes formed upon interaction of the receptors with different ligands, which in turn has been shown to correlate with activation of the IKK complex and NF-κB activation (Cruz et al., 2021). Modeling suggested that the limiting factor in the activation of NF-κB in response to TNF-α and Il-1β is the abundance of cognate receptor; the abundance of signal transducers is in large excess relative to receptors and hence is not the limiting factor in NF-κB activation. Our transcriptome-constrained estimations indicated that the ranking of clone responsiveness to IL-1β and TNF-α would be different, and experimental evidence confirmed the prediction. Notably, the notion

that the abundance of receptor transcripts can be used to predict responsiveness also holds for other systems (Su et al., 2022).

We also show here how differences upstream of NF-κB, combined with the expression levels of the component of the main negative feedback of NF-κB (IκBα), predict whether the NF-κB response will be sharp or persistent. Furthermore, the experimental data show that a moderate reduction in IκBα level induced by antisense oligonucleotides can lead to relatively large differences in the NF-κB dynamics. Consistently, knock-out of IκBα gene *Nfkbia* has been shown to induce a change from oscillatory to sustained dynamics (Cheng et al., 2021; Adelaja et al., 2021).

Part of the success of our approach is probably due to the biological homogeneity of the clones, which derive from cells of the same type that come from a single embryo. We assume that differences in the transcriptional levels between our cell populations are informative of differences in the protein levels; while this is not necessarily true for any two cell populations, we expect it to hold for quasi-identical cell populations. We hypothesize that a similar analytical approach could be used to predict the relative difference in the dynamic response of other TFs in other relatively homogeneous cell populations, as for example in cells derived from the same tissue or in clones within a tumor mass (Greaves and Maley, 2012) that might respond differently to therapy (Paek et al., 2016).

NF-κB oscillatory phenotype is fuzzy. NF-κB nuclear localization dynamics in single living cells was observed for the first time more than 15 years ago (Nelson et al., 2004) and since then its oscillatory nature was subject to discussion (Barken et al., 2005; Nelson et al., 2005). More recently, we argued that NF-κB displays damped oscillations (Zambrano et al., 2016) as compared to the sustained oscillations reported by others (Kellogg and Tay, 2015). Our present work shows that classification of NF-κB dynamics is not necessarily binary. Within a population of quasi-identical cells, we can find subpopulations of cells that are more and less prone to oscillate. For circadian oscillators as well it was found that clonal populations have different oscillatory features (Li et al., 2020). For our cells, we show that this largely depends on the expression level of genes belonging to the NF-κB regulatory circuit. If small transcriptional differences can affect the dynamics of NF-κB, it is not surprising that different cell types have completely different oscillatory phenotypes.

Stimulus specificity in the NF-κB response is clone-dependent. The increasing availability of single-cell data on NF-κB dynamics has shown that it is possible for cells to discriminate between stimulus type (Adelaja et al., 2021; Cheng et al., 2021; Martin et al., 2020), dose (Tay et al., 2010; Zambrano et al., 2014; Q. Zhang et al., 2017) and dynamic profile (Ashall et al., 2009; Lee et al., 2016; Zambrano et al., 2016). Here, we find that two MEF clones from the same embryo, clone G and clone B, do respond differently to two different stimuli: clone G responds strongly to IL-1β, while clone B responds strongly to both TNF-α and IL-1β. On the other hand, clone R produces a sharper and more oscillatory NF-κB response than clone B. This indicates that stimulus specificity in NF-κB dynamics is clone-dependent and, all the more so, that it will vary among cell types within the same organism. This is in line with a recent study shows that a synthetic version of the NF-κB system ectopically expressed in yeast (Zhang et al., 2017) displays different types of dynamics and responses by manipulating the expression of key genes

within the genetic circuit. Furthermore, since immortalized MEFs maintain certain characteristics of primary MEFs (Beg and Baltimore, 1996), our work suggests that a similar fine-tuning can take place naturally in primary mammalian cells; although recently developed reporter mice (Rahman et al., 2022) have allowed to show that primary cells and cell lines can have different NF-κB dynamical features. Only further analysis of primary cells will allow us to address this question.

Origin of the transcriptional differences across clones. We show that the dynamical differences observed between clones are robust and persist over time and cell culturing. Our bioinformatic analysis could not detect any variant among clones in the coding sequence of genes involved in the NF-κB response. We inferred a substitution rate in the genome of the clones in the order of $5 \cdot 10^{-7}$ per base pair, which would translate to <100 substitutions per haploid genome. This substitution rate is consistent with somatic variability of cells from the same organism (Amand et al., 2016; Milholland et al., 2017). However RNA-sequencing based analysis cannot detect other genetic changes, such as sequence changes in the regulatory regions or copy number variations. These could well lead to the small (although robust) differences in gene expression reported here. The other possibility is epigenomic variation between different cells, i.e. in DNA methylation or chromatin accessibility of gene control elements. We find that the most visible difference in the transcriptomics of the different clonal populations is related to developmental programs, which indeed involve epigenetic variations. Whether expression of different developmental programs can give rise to the difference in expression of the genes that affect the NF-κB dynamic response remains to be proved, but we speculate that this is at least likely.

Cell to cell differences within clones. We find that the NF-κB dynamic response of the cells within each clonal population is still heterogeneous. We speculate that this cell-to-cell variability can have a purely stochastic component related to the probabilistic nature of the activation of gene transcription. Indeed, we recently found experimentally that even highly transcribed genes under the control of NF-κB like the one encoding for IκBα are transcribed stochastically (Zambrano et al., 2020). Thus, the same cell might be oscillatory or not at different times, depending on how recently it had a burst of IκBα transcription and translation. Future studies will be needed to connect the transcriptional history of each single cell with its NF-κB dynamics.

In sum, our work shows that part of the NF-κB dynamic heterogeneity observed within a relatively homogenous population of cells can be due to small (less than twofold) differences in the expression levels of genes belonging to the NF-κB signaling pathway. However, some heterogeneity remains between cells of the same clone, which we suggest might be due to noisy transcriptional bursts in individual cells. We speculate that analogous mechanisms might also diversify the dynamic response of other TFs to external cues.

ACKNOWLEDGEMENTS

We acknowledge Prof. Manolis Pasparakis for sharing with us the immortalized MEF population from a single embryo, Prof. Roberto Sitia for suggesting the initial experiment and Davide Mazza for critical revision of the manuscript. We received funding from Ospedale San Raffaele (OSR Seed Grant to S.Z.), San Raffaele University (predoctoral fellowship to C.K.) and Associazione Italiana Ricerca sul Cancro (AIRC 2017-ID.18687, project PI A.A). Part of the present work was performed by CK in partial fulfillment of the requirements for obtaining the PhD degree at Vita-Salute San Raffaele University, Milano, Italy.

AUTHOR CONTRIBUTION

Conceptualization: SZ. Supervision: SZ, MEB, AA. Visualization: SZ, CK, EM, MEB. Formal Analysis: CK, SZ, EM, AA. Investigation: CK, SZ, EM, JGM, FB. Writing-Original draft: SZ, CK, MEB Writing-review and Editing: SZ, CK, EM, MEB, AA, JGM, FB. Funding acquisition: SZ, MEB, AA.

DECLARATION OF INTERESTS

The authors declare no competing interests.

FIGURE LEGENDS

Figure 1. Clonal populations derived from a population of MEFs derived from a single embryo have distinct dynamics upon TNF-α. A. Representative images of the heterogeneous response to 10 ng/ml TNF-α of our initial population of MEFs, the pool. **B.** Heterogeneous NF-κB dynamic profiles of four cells from our MEFs population including weak, oscillatory and persistent responses to 10 ng/ml of TNF-α. **C.** The dynamic heatmap of the pool, which represents the NF-κB dynamics of hundreds of cells sorted by their maximum NCI value. **D.** Single cell cloning strategy of our initial population of MEFs (referred to as "pool"). Clones were expanded and used for live cell imaging. **E.** Dynamic heatmaps of eight clones isolated from our population (Clones B, R and G are highlighted). **F.** The color-coded plot shows co-clustering probability of NF-κB dynamic profiles of each population considered (8 clones and the pool) based on an unsupervised k-means clustering. **G.** Distribution of the values of an entropy-like disorder parameter calculated for each realization of the stochastic clustering for the original dataset versus a randomized one. The distributions do not overlap in 500 realizations of the stochastic clustering for the original and the randomized datasets, $p<2\cdot10^{-3}$.

Figure 2. Clones B, R and G have distinct responses to TNF-α and are oscillatory to different degrees. A. Representative images from our time-lapse movies for clones B, R and G upon 10 ng/ml TNF-α stimulation. **B.** NF-κB dynamic response of the clones to TNF-α as assessed by the average NCI. **C.** The boxplots show the dynamical features of the response to TNF-α: NCI value of the first peak, timing of the first peak and area under the curve (AUC) in each population. **D.** Examples of NCI profiles with 1, 2 and 3 peaks (top, lighter to darker colors) and frequency of the number of the oscillatory peaks observed (bottom) for each population in 4 hours. **E.** Periods of the oscillations computed as the inter-peak timing for each population. **F.** Ratios of the oscillatory peak values for each clonal population. In all panels $*p<10^{-2}$, $** p<10^{-3}$,$*** p<10^{-4}$, multiple comparisons through Kruskal-Wallis.

Figure 3. Clones B, R and G have distinct transcriptional programs. A. Scheme of the RNA-sequencing performed: 5 replicates per population, treated 1 hour with 10 ng/ml TNF-α or untreated (UT). **B.** PCA of the UT and TNF-α treated samples of our clones B, R, G and the pool, considering all genes. **C**. Gene ontology analysis of the differentially expressed genes between the clonal populations. **D.** PCA considering only NF-κB targets. **E.** Volcano plots of gene expression upon TNF-α for clone B, R and G (each dot is a single gene). **F.** Fold change expression of differentially upregulated genes in clone B, R and G. *$p<10^{-2}$, ** $p<10^{-3}$,*** $p<10^{-4}$, multiple comparisons through Kruskal-Wallis.

Figure 4. Transcriptomic-constrained predictions show the number of activating complexes formed upon TNF-α correlates with clones' response. A. Scheme depicting the formation of the Complex I upon interaction of TNF-α with its receptor, leading to the IKK kinase complex activation. **B.** Expression level of the gene encoding for TNFR1 for the untreated clones, error bars display mean and standard deviations, each dot is a replicate. **C.** Scheme of the transcriptomic-constrained prediction scheme of the number of complexes formed for different values of Δ (differences in order of magnitude between copies of TNFR1 and rest of the proteins in the complex) and dissociation constant K_D. **D.** Transcriptomic-constrained prediction of the fold change (FC) in the number of activating complexes formed upon TNF-α in clones B vs R (blue) and in G vs R (green) for the experimentally observed value Δ=3 and different maximum values of K_D considered in the simulations. Thick solid lines indicate the mean of the simulations, thin lines and shaded areas represent the standard deviation. **E.** Transcriptomic-constrained prediction of the FC in the number of activating complexes formed upon TNF-α in clones B vs R (blue) and G vs R (green) in the limit K_D=0. Solid lines indicate the mean of the simulations, thin lines and shaded areas represent the standard deviation. **F.** Scheme of the NF-κB genetic circuit with main negative feedback regulators and including explicitly the number of activating complexes formed. **G.** Simulations of our mathematical model for a range of activating complex numbers and plot of the resulting NF-κB response for each value (inset), red line and red dot correspond to the same simulations. **H.** Result of fitting the FC in the number of activating complex needed in B vs R and G vs R to reproduce the differences in the NF-κB responses to TNF-α observed, for different realization of the remaining model parameter values. *$p<10^{-2}$, ** $p<10^{-3}$,*** $p<10^{-4}$, one-way Anova.

Figure 5. Transcriptomic-constrained simulations predict differences in the clones' response to IL-1β. A. Scheme depicting the formation of the activating complex arising upon interaction of IL-1β with its dimeric receptor. **B.** Expression level of the gene encoding for IL-1R3 for the untreated clones, error bars display mean and standard deviations, each dot is a replicate. **C.** Transcriptomic-constrained prediction of the FC in the number of activating complexes formed upon IL-1β by clones B vs R (blue) and G vs R (green) for the experimentally observed value Δ=3 and different values of K_D considered in the simulations (the most abundant proteins can have up to 10^6 copies in the simulations). Thick solid lines indicate the mean of the simulations, thin lines and shaded areas represent the standard deviation. **D.** Transcriptomic-constrained prediction of the number of activating complexes formed upon IL-1β by clones B vs R (blue) and G vs R (green) in the limit K_D=0. Solid lines indicate the mean of the simulations, shaded areas within thin lines represent the standard deviation. **E.** Results of fitting the FC in the number

of activating complex needed in B vs R and G vs R to reproduce the differences in the NF-κB responses to IL-1β experimentally observed, for different randomizations of the remaining parameter values. **F.** Dynamic heatmap of the responses of clone B, R and G to 100 ng/ml IL-1β. **G.** Average NF-κB response for the three clones upon IL-1β stimulation. **H.** The boxplots show the dynamical features of the response to IL-1β: value of the first peak, timing and area under the curve (AUC). **I.** Examples of NCI profiles with 1 , 2 and 3 peaks (top, lighter to darker colors) and frequency of the number of the oscillatory peaks observed for each clonal population (bottom) in 4 hours upon IL-1β. **J.** Periods of the oscillations computed as the inter-peak timing for each population. *$p<10^{-2}$, ** $p<10^{-3}$,*** $p<10^{-4}$, multiple comparisons through Kruskal-Wallis.

Figure 6. Differences in expression levels of NF-κB negative feedbacks can reproduce the observed dynamical differences between clones. A. Resulting change in the AUC of the clone B against clone R when fitting the number of activating complex needed to match the differences in their NF-κB responses to TNF-α and IL-1β for different combinations of the remaining parameter values, and experimental estimate of the average difference (dashed gray). **B.** Expression level of the gene encoding for IκBα (*Nfkbia*) for clones after 1 hour of TNF-α, error bars display mean and standard deviations, each dot is a replicate. **C.** *Nfkbia* levels of our transcriptionally constrained numerical simulations of clone R and clone B, each dot is a single simulation using parameters from a randomization. Dashed line indicates the experimentally observed ratio, solid black line is the identity. **D.** Exemplary simulations with the imposed change in *Nfkbia* levels shown in C (dashed) leading to a change in the dynamics (solid line) in the simulations of R versus B. **E.** Changes of the AUC resulting of changing the following model parameters, following the experimental data: the amount of NF-κB, both the amount of NF-κB and the number of activating complexes to fit the NF-κB response, and the two previous combined with the amount of *Nfkbia*, for different randomization of the model parameters. Dashed line shows experimentally determined difference in the average AUCs between B and R upon TNF-α. **F.** Change in the number of peaks for simulations giving oscillatory profiles (at least 2 peaks), when only the number of activating complexes and the NF-κB amount are changed (top), and also when the amount of *Nfkbia* is changed (bottom). **G.** Representative dynamic heatmaps of clone B and clone R upon TNF-α for both untreated and ASO-treated cells. **H.** Quantification of the maximum response for untreated and ASO-treated cells upon TNF-α. **I.** Quantification of the AUC for untreated and ASO-treated cells upon TNF-α. **I.** Simulated effect of modulating *Nfkbia* in the response and the AUC of different randomizations of the model's parameters, dashed line indicates experimentally observed changes. *$p<10^{-2}$, ** $p<10^{-3}$,*** $p<10^{-4}$, multiple comparisons through one way Anova (panel E) and Kruskal-Wallis (remaining panels).

METHODS

Cell line and cell culture. GFP-p65 knock-in mouse embryonic fibroblasts (MEFs) were kindly provided by M. Pasparakis. MEFs were derived from a single embryo of a homozygous knock-in GFP-p65 expressing mouse model, using standard protocols (De Lorenzi et al., 2009) and immortalized by serial passaging following the "3T3 method" that typically involves 20-30 passages (Amand et al., 2016). Clones were generated from a freshly frozen vial of these MEFs, and aliquots of each clone were frozen and then used

for few passages, to keep at a minimum the number of passages. The cells were cultured in phenol-red free DMEM supplemented with 10% FCS, 50 mM b-mercaptoethanol, 1x L-glutamine, 1x pen/strep, 1x sodium pyruvate and 1x non-essential amino acids. MEFs were subcultured every 2-3 days before they reached 100% confluency and kept at 37°C and 5% CO2.

Generation of the clonal populations by single cell cloning. MEFs were harvested by 1x Trypsin solution and counted. Final concentration of 5 cells/ml was achieved by serial dilutions and 100 µl of the cell suspension per well were pipetted to a 96-well plate. The plate was screened for single colonies and selected colonies were then expanded.

Cell treatments. Where indicated the cells were stimulated with the final concentration of 10 ng/ml of recombinant human TNF-α protein (R&D Systems) or 100 ng/ml of recombinant human interleukin 1 beta (IL-1β, PeproTech).

Live cell imaging. Live cell imaging of GFP-p65 knock-in MEFs was performed as in (Zambrano et al., 2016). We used a Leica TCS SP5 confocal microscope with an incubation system where cells were stably maintained at 37°C in 5% CO2. Time-lapse images were acquired at 6 min intervals for up to 10 hr. We used a low magnification objective (20x, 0.5 NA) and an open pinhole (Airy 3), ensuring that the image depth (10.7 µm) contains the thickness of the whole cell so that images capture the total cell fluorescence. GFP-p65 is imaged with the 488 nm Argon laser (GFP channel) while Hoechst 33342 stained nuclei are imaged with the low energy 405 nm UV diode laser at 5% of its maximum intensity (HOE channel). The staining was performed at room temperature for 10-15 minutes using NucBlue™ (Live ReadyProbes™ Reagent, ThermoFischer), 1:100 v/v and incubated 10-15 min at RT. We showed previously in this same cell line that imaging and staining do not interfere with the response to TNF-α, the cell's viability and ability to replicate (Zambrano et al., 2016), so we exclude any relevant phototoxicity effects of our imaging. Images were acquired as 16 bit, 1024×1024, TIFF files. Experiment replicates were performed on different days. In each experiment we typically imaged more than one clone in different wells of an 8-well labtek.

Automated quantification of NF-κB dynamics in single living cells. To quantify NF-κB nuclear localization dynamics in living cells, we follow our previously described procedure of normalizing the average nuclear signal intensity by the average cytosolic fluorescence intensity (Zambrano et al., 2016) to obtain the nuclear to cytosolic intensity (NCI), also used by others (Kellogg and Tay, 2015; Paszek et al., 2010). We improved our custom-made routines that run on Matlab R2015 and are made available online. In short, nuclei are segmented based on the intensity of the HOE channel, and nuclear masks are used to compute the nuclear average NF-κB intensity in each cell. In order to estimate the average cytoplasmic NF-κB intensity, first the background was computed by taking a square area centered on the cell nucleus, dividing it in tiles and using the one with the smallest average intensity in the GFP channel. After this, pixels belonging to the cytoplasm are those with intensity above the background on a ring around each nucleus of width 0.5 times the nuclear radius. Tracking of cells between frames is performed through an optimized algorithm based on the Hungarian linker method (Careccia, 2019). Cells are discarded upon abrupt changes of the nuclear and/or cytosolic areas, indicative of erroneous tracking or cell death or

mitosis. The resulting NCI profiles, that we refer to as NF-κB dynamic profiles, where smoothened using the Matlab function *smooth*.

Stochastic clustering of the* NF-κB *dynamic profiles. We performed an unsupervised clustering of NF-κB dynamic profiles from cells of the 8 clones and the pool using the k-means algorithm (k=9) implemented on (Matlab) and based on the euclidean distance between profiles. Since we have hundreds of cells per clone, in each realization we randomly picked 50 profiles from each population. The profiles are clustered then in 9 groups (**Figure S1B**), and we compute the number of cells from each clonal population in each cluster (**Figure S1C**). In each realization we compute p_{ik}, representing the fraction of trajectories of clone *k* that are present in the cluster where the clone *i* has a higher number of clustered profiles. For *k=i*, it represents the fraction of cells of the clone *i* in the cluster where it is more represented. The result for a single realization is shown in **Figure S1D**, the average of many realizations is on **Figure 1G**. For 500 realizations we computed the disorder parameter defined as $S = -\sum_{i,j} p_{ij} \log p_{ij}$. For each of them we repeated the procedure but randomly assigning the selected profiles to the 9 populations, and calculating for each clustering the disorder parameter. The disorder parameter was always higher for cells randomly assigned to the populations, indicating further that NF-κB dynamic profiles are clustered prevalently according to the clonal population of origin.

Analysis of NF-κB dynamics. To extract the dynamic features of the NCI time series we followed the same procedure as in (Zambrano et al., 2014, 2016). In short, NCI series are smoothed and peaks are detected using standard Matlab functions (*smooth* and *findpeaks*, respectively) and those with a prominence θ>0.15 are considered real peaks. This value is well beyond the prominence of noisy peaks found in this type of datasets (Zambrano et al., 2016) and provides a reasonably good compromise between the need to ignore noise peaks and the need to detect small peaks of valuable dynamical information (e.g. to classify an NF-κB dynamic profile as oscillating or not). The timing of the peak was determined considering the maximum value. Instead, the area under the curve is calculated as the integral in the time interval considered of NCI(t).

Cell cycle analysis. Cell cycle analysis was done as described in (Brambilla et al., 2020): MEFs were harvested and fixed with cold 70% ethanol and kept overnight at -20°C. Cells were then washed once with 5% FBS/PBS and stained with PBS containing 10 µg/ml propidium iodide and 10 µg/ml RNAse A for 1 hour at room temperature. Samples were then read at a cytometer using a 488 nm laser.

Cell cycle computational correction: Clone B has a stronger response than clone B, and it has a higher fraction of cells in the S-phase. This could be the source of the stronger response in clone B so, to computationally correct for this, we generated an artificial cell-cycle corrected dataset of NCI time series of clone R where the time series where sorted by their response and the top 25% of the population was assumed to be the S-phase high responders (Ankers et al., 2016). To increase their percentage to 43% (as clone R) we discarded 42% of the profiles, those of lower responses, to "match" the fraction of cells in S-phase in clone B (see Table 1). The resulting dataset has a higher AUC value than the original but still

a lower value of the AUC than clone B (**Figure S2J**) which makes it unlikely that cell cycle is the key driver of this inter-clonal difference. Furthermore, clones B and G have very similar cell cycle distribution and even so their dynamics upon TNF-α are markedly different, as detailed in the main text.

RNA isolation and real time PCR. $1.5x10^5$ MEFs were plated on a 6-well plate a day before the extraction. Total RNA was isolated using the NucleoSpin RNA II kit (Macherey-Nagel). The amount of RNA was determined using a NanoDrop spectrophotometer (Thermo Fisher Scientific) and 1 μg was then reverse transcribed using SuperScript IV Reverse Transcriptase (Thermo Fisher Scientific). qPCR was performed using LightCycler 480 SYBR Green I Master (Roche). The expression of *IκBα* was checked using following primers:
IκBα forward: 5' CTTGGCTGTGATCACCAACCAG 3'
IκBα reverse: 5' CGAAACCAGGTCAGGATTCTGC 3'
A20 forward: 5' ACAGAGCAGGGACAAGCAAGTG 3'
A20 reverse: 5' GTTTAGGGGGCTCTTCAGGC 3'

RNA sequencing and Bioinformatic analysis. Libraries for Illumina NGS were prepared as described in (Brambilla et al., 2020). After trimming the adapter sequences (cutadapt, https://cutadapt.readthedocs.io) reads were mapped to mouse genome (mm10) using hisat2 (http://daehwankimlab.github.io/hisat2/) using parameters "-p 20 -5 5".
Read counting was performed using featureCounts from the Subread Package and features displaying less than 10 reads were filtered out. Differential expression analysis was performed using DESeq2 (https://bioconductor.org/packages/release/bioc/html/DESeq2.html) with the following design formula "=~ 1 + clone + treatment + clone:treatment".
Principal component analysis (PCA) was performed using Matlab, keeping only genes for which RPKM>1 in at least five samples. Additional RNA-seq datafrom several mouse tissues were retrieved from the ENCODE Database (https://www.encodeproject.org). Volcano plots were generated using Matlab and p-values derived from the t-test statistics. Gene ontology was performed using the "*clusterProfiler*" R package (https://bioconductor.org/packages/release/bioc/html/clusterProfiler.html). Heatmap and hierarchical clustering was performed using the "*Pheatmap*" R package.
Genes annotated in the mouse TNF-signalling were retrieved from WikiPathway (https://www.wikipathways.org/index.php/Pathway:WP246)

ssGSEA analysis: Genes from the "TNF-α to NF-κB" and "IL-1β to NF-κB" lists were ranked according to their log normalized expression (log2 FPKM + pseudocount) and for each biological replicate (n=5), normalized enrichment scores (NES) were calculated (Barbie et al., 2009). The NES reflects the degree to which the gene list is coordinately up or down-regulated within each clone.

Estimation of the genetic differences between clonal populations. The SNP calling step was performed using the GATK 3.6 toolkit. (McKenna A et., 2010) in order to split splice junction reads, to recalibrate quality scores and to call variants. To minimize false positive variants the GATK Variant filtration tool was used using the following parameters:

"--filterExpression QD < 5.0 --filterExpression DP < 10 --filterExpression ReadPosRankSum < -8.0 --filterExpression MQRankSum < -12.5 --filterExpression MQ < 40.0 --filterExpression FS > 60.0". Nucleotide positions with heterozygosity scores < 0.10 were excluded as previously described (Adetunji et al., 2019).

We called SNPs with different levels of confidence based on three different coverage cut-offs (5x, 10x, 20x) and then we calculated the number of unique SNPs for each clone. We find that our clones differ in a range of 200-400 nucleotides (**Table 2**) which, once divided by the length of the genome at the specific coverage cut-off, provided us a "mutation rate" of approximately $5 \cdot 10^{-7}$ per base pair (**Figure S3B**). Interestingly, this is of the order of magnitude of the somatic mutation rate found between somatic cells from the same mouse (Milholland et al., 2017) indicating how the frequency of SNPs for our clones correspond to "somatic differences" that can be found between cells of the same organism. Of note, our cells come from the same embryo and immortalization by serial passages requires a few dozen cell replications (Amand et al., 2016; Todaro and Green, 1963). Moreover, no mutations on NF-κB-related genes of the *wikipathways* database were identified.

Complex formation simulations and estimation of the equilibrium concentrations

To estimate the differences between clones in the number of activating complexes formed after interaction between ligand and the receptor we describe their formation as a sequence of association-dissociation reactions. For the sake of simplicity, and considering also experimental data on the dynamics of complex formation (Cruz et al., 2021), we consider that those reactions take place very quickly compared with NF-κB response, so their equilibrium concentration is the only relevant magnitude to determine the short-term NF-κB response.

To evaluate the equilibrium concentrations, we make the following considerations. Each reaction of the formation of a complex $(A{:}\,B)$ of biochemical species A and B can be written as:

$$A + B \leftrightarrow (A{:}\,B)$$

While the evolution in time of the number of copies of each species, that we represent with the same letters, is given by

$$\frac{dA}{dt} = -\,k_a \cdot A \cdot B + k_d \cdot (A{:}\,B) \quad \text{(i)}$$

$$\frac{dB}{dt} = -\,k_a \cdot A \cdot B + k_d \cdot (A{:}\,B) \quad \text{(ii)}$$

$$\frac{d(A{:}B)}{dt} = k_a \cdot (A{:}\,B) - k_d \cdot A \cdot B \quad \text{(iii)}$$

Where k_a and k_d are the association and dissociation rates, respectively, of the species to form the complex. If we denote by A_0 and B_0 the total amount of the biochemical species A and B (the sum of

the free and the complex-forming ones), the equilibrium concentrations A_{eq}, B_{eq} and $(A{:}B)_{eq}$ satisfy the equations:

$(A{:}B)_{eq} + A_{eq} = A_0$ (iv)

$(A{:}B)_{eq} + B_{eq} = B_0$ (v)

$A_{eq} \cdot B_{eq} = K_D \cdot (A{:}B)_{eq}$ (vi)

Where $K_D = k_d/k_a$ is the dissociation constant. If we specify the species amounts in number of molecules, K_D is also given in number of molecules (when specified in concentrations, the dissociation constant has units of concentration).

It is relatively easy to see that the equilibrium concentrations can be found solving a second-degree equation. In **Figure S4D** we show simulations of this system in which we consider that $A(0) = A_0$, $B(0) = B_0$ and hence $(A{:}B)(0) = 0$, showing how they all converge to the equilibrium values computed solving (iv)-(vi). The panels in **Figure S4D**, from left to right, show the evolution of the species towards equilibrium in a situation where $B_0 < A_0$: if $K_D = 0$, then $(A{:}B)_{eq} = B_0$ (the smaller abundance) ; if $K_D \ll B_0$ then $(A{:}B)_{eq} \simeq B_0$; if $B_0 \leq K_D \leq A_0$ then also $B_0 \leq (A{:}B)_{eq} \leq A_0$ and finally if $K_D \gg A_0$, $(A{:}B)_{eq} \simeq 0$. Reasoning along these lines, it is easy to see that in the process of association of many species to form a complex, the upper bound of the number of complexes is given by the less abundant species.

Transcriptomic-constrained estimation on the number of activating complexes in the clones upon stimuli.

The formation of the Complex I upon TNF-α stimulation (DeFelice et al., 2019; Hayden and Ghosh, 2008; Hsu et al., 1996; Lee et al., 2016; Wilson et al., 2009) or what we call here the "activating complex for TNF-α", can be represented as the following biochemical reactions:

TNF-α + TNFR1 ↔ C_1

C_1+ TRADD ↔ C_2

C_2 + RIP1 ↔ C_3

C_3+ TRAF2/5 ↔ C_4

C_4+cIAP1/2 ↔ C_5

TAK1+TAB1/2 ↔ TAK1:TAB1/2

C_5 + TAK1:TAB1/2 ↔ $C_{TNF\text{-}\alpha}$

Notice that we denote the complex emerging from the addition of a new element as C_n for the sake of simplicity. The final activating complex is $C_{TNF\text{-}\alpha}$. The list of the genes coding for the proteins involved in the reactions, our "TNF-α to NF-κB" list, is : *'Tnfrsf1a', 'Tradd', 'Ripk1', 'Traf2', 'Traf5', 'Birc2', 'Birc3', 'Map3k7', 'Tab1', 'Tab2'.*

Analogously, the activation of NF-κB upon IL-1β follows the formation of its own activating complex upon the interaction of the dimeric receptor with its ligand: following the reactions (Martin et al., 2020; Rhyasen and Starczynowski, 2015):

IL-1R1 + IL-1R3 ↔C_1

IL-1β +C_1 ↔C_2

C_2 + MyD88 ↔C_3

C_3 +TOLLIP ↔ C_4

C_4 + IRAK1 ↔ C_5

C_5 + TRAF6 ↔ C_6

C_6+ TAK1 ↔ C_7

C_7 + TAB1/TAB2 ↔ $C_{IL\text{-}1\beta}$

The list of the genes coding for the proteins involved in the reactions, our "IL-1β to NF-κB" list, is: '*Il1r1*';'*Il1rap*';'*Myd88*';'*Irak1*';'*Map3k7*';'*Traf6*';'*Tab1*';'*Tab2*'. The activating complex is denoted by $C_{IL\text{-}1\beta}$.

The description above is a simplification where we have deliberately neglected the precise stoichiometry of each reaction (which in some cases is not so clear); however, we implemented also simulations using other stoichiometries postulated in the literature with analogous result (easily reproducible with the software provided).

In principle, if we knew the copy number of each protein and the dissociation constant of each of the association-dissociation reactions above, we shall be able to determine the abundances of the complexes $C_{TNF\text{-}\alpha}$ and $C_{IL\text{-}1\beta}$ (in equilibrium, which we assume to happen fast). However, we do not know

them, but we can make simulations to compute how their numbers compare between clones under reasonable assumptions:

- First, we assume that clonal populations have similar translation rates and protein degradations for each protein, so the ratios between the amount of transcript and protein of each species should be similar. Since we have 5 replicates of each condition, we consider that for each simulation we have 5 values of the relative protein abundance for each protein involved. This also provides us with an experimental error that will contribute to the uncertainty of our estimates.

- Second, we know that there is a difference in the order of magnitude of the number of copies between certain proteins in these reactions and the remaining ones; in particular the protein copies of TNFR1 are about $\Delta \gtrsim 3$ orders of magnitude less abundant than the other proteins leading to $C_{TNF\text{-}\alpha}$ ($O(10^3)$ vs $O(10^6)$), and IL-1R3 proteins are about one order of magnitude less abundant than ILR1 and $\Delta \gtrsim 4$ orders of magnitude less abundant than the remaining proteins leading to the complex $C_{IL\text{-}1\beta}$ ($O(10^2)$ vs $O(10^4)$) (Cruz et al., 2021; Hwang et al., 2015). These receptor proteins will act as limiting factors in the abundance of the complexes.

Under these two assumptions, we can make estimates of the activating complex abundances $C_{IL\text{-}1\beta}$ and $C_{TNF\text{-}\alpha}$ for each clonal population by randomizing the proportionality between the copy numbers of each protein species, but preserving the ratios between expression in the clones specified by transcriptomic data. Estimations are performed using experimentally determined Δ values but also different ones to test for robustness. We also use different K_D values, picked randomly up to a value indicated in the simulations (we considered at most the maximum protein abundance, 10^6). Once randomized, one can calculate reaction by reaction the equilibrium concentrations C_n in a sequential way, using the same numerical tools described in the previous section, up to $C_{TNF\text{-}\alpha}$ and $C_{IL\text{-}1\beta}$. The ratios of the resulting copy numbers between clones are then informative of the expected FC difference in copy numbers of the activating complex between each of them. These values will be different in each simulation of these transcriptomic-constrained simulations, but we can find their mean value and its standard deviation for given K_D and Δ values.

It is worth discussing two limit cases. First, for large Δ values in principle the ratios between the numbers $C_{TNF\text{-}\alpha}$ and $C_{IL\text{-}1\beta}$ will be dominated by the ratios of the less abundant proteins in the simulations, which in turn will be proportional to the ratios of the RNA expression. We indeed find that this convergence takes place really fast for values of Δ much smaller than the experimentally estimated ones if the values of K_D are moderate (e.g. **Figures 4E** and **S4E**, **Figures 5D** and **S5D**). Second, for large K_D values (comparable to the copy number of the proteins considered here ($O(10^6)$) we might expect that some step of the complex formation reactions will lead to a very small number of resulting complexes (consider the simple two species case of **Figure S4D**). This results in a high variability in the number of complexes estimated for large K_D as we observe in **Figure S4F** and **Figure S5F**. Those panels show how such variability is mitigated for sufficiently large Δ by the mathematical reasoning sketched above.

Mathematical model of NF-κB signaling. We use here a slightly modified version of our model of NF-κB dynamics (Zambrano et al., 2014, 2016), that we briefly describe below.

As described in different works and experimentally observed, NF-κB activation follows the formation of a number of activating complexes C downstream the ligand-bound receptor, where the kinase complex IKK is activated proportionally to the amount of activating complex formed C upon stimuli ($C_{TNF-\alpha}$ or $C_{IL-1\beta}$) through the constant k_0. Hence the evolution of the abundance of the active IKK complex, that we denote K, can be written as:

$$\frac{dK}{dt} = \frac{k_0 \cdot C \cdot S}{(1+\left(\frac{A}{A_0}\right)^n)} - d_K \cdot K$$

The amount of activating complex is regulated by the amount of the protein A20, that we denote A, through a hill function of parameters A_0 and n, and will also depend on the inactivation rate of the kinase complex d_K and the presence ($S = 1$) or absence ($S = 0$) of the external inflammatory signal. Importantly, this simple model of kinase activation reproduces the linear relationship between number of complexes C and NF-κB response (measured as maximum of the nuclear to cytosolic NF-κB intensity, **Figure 4G**), in agreement with what has been observed experimentally (Cruz et al., 2021) .

In this new model, the amount of free nuclear NF-κB, N, depends on its continuous association-dissociation with the IκBα inhibitor protein, whose abundance we represent as I, to form the complex (cytosolic) form $(N{:}\,I)$. The active kinase can degrade the inhibitor in the complex, so:

$$\frac{dN}{dt} = - k_a \cdot N \cdot I + k_d \cdot (N{:}\,I) + d_C \cdot (N{:}\,I) + d_K \cdot K \cdot (N{:}\,I)$$

Where k_a and k_d are the association and dissociation rates, respectively, d_K is the degradation rate of the inhibitor in $(N{:}\,I)$ due to the presence of the active kinase, while d_C is the spontaneous degradation of the inhibitor in $(N{:}\,I)$. The evolution of the complex abundance is given by:

$$\frac{d(N{:}I)}{dt} = k_a \cdot N \cdot I - k_d \cdot (N{:}\,I) - d_C \cdot (N{:}\,I) - d_K \cdot K \cdot (N{:}\,I)$$

So the total amount of NF-κB (free plus bound) is constant $N + (N{:}\,I) = N_0$.

For the free inhibitor, beyond the association and dissociation with NF-κB, the evolution will depend also on the translation rate k_I of the available mRNA, that we denote as R, and on the inhibitor's own protein degradation rate d_I so:

$$\frac{dI}{dt} = - k_a \cdot N \cdot I + k_d \cdot (N{:}\,I) - d_{IK} \cdot K \cdot I + k_I \cdot R - d_I \cdot I$$

The mRNA expression level of the mRNA amount R is summarized in the following equations that model the first main negative feedback of the system, determined by the level of activity of the gene G coding for the inhibitor:

$$\frac{dR}{dt} = k \cdot G - \delta \cdot R$$

$$\frac{dG}{dt} = k_{on} N \cdot (2 - G) - k_{off} \cdot G$$

where δ is the degradation rate of the mRNA and k is the transcription rate, while and k_{on} and k_{off} are the gene activation-inactivation rates respectively.

The amount of A20, the second negative feedback of the system that operates upstream and we denote as A, is governed by an analogous set of equations that encode for the time evolution of its protein abundance, A, its available mRNA, that we denote as R_A, and on the activity of the gene encoding for it, that we denote G_A:

$$\frac{dA}{dt} = k_{t,A} \cdot R_A - d_A \cdot A$$

$$\frac{dR_A}{dt} = k_A \cdot G_A - \delta_A \cdot R_A$$

$$\frac{dG_A}{dt} = k_{on,A} N \cdot (2 - G_A) - k_{off,A} \cdot G_A$$

With its own parameters governing gene activation/inactivation, transcription and translation kinetics, in an analogous way to the parameters of the IκBα feedback. The starting parameters of the model are specified in Table 3.

Experimentally constrained mathematical modeling of NF-κB dynamics.

In the paper we perform numerical simulations constrained by our experimental data in different ways, to assess to what extent certain experimental differences observed between clones B, R and G can explain the different dynamic responses obtained. In all of them we use the same rationale: we fix the parameters of our model that reproduces the dynamics of clone R, and then we adjust only certain parameters (those suggested by certain experimental observations) to see if this is enough to reproduce the differences effect in the NF-κB dynamics observed with respect to the other clones (B and G). To be sure that this analysis on the impact on NF-κB dynamics of certain(s) experimentally observed differences between clones does not depend on the initial choice of parameters, this operation is typically repeated by randomizing the parameters of the model up to a factor 2 to generate different "randomizations of clone R" that are taken as a starting point, on which we apply the experimentally-derived corrections. We describe those corrections below.

Modulating NF-κB amount. A first simple example is that of **Figure S4G** where we perform a simulation with the parameters specified in the Table 3 to obtain a simulated trajectory of clone R (red line), and then we perform new simulations by changing the NF-κB amount in our model (N_0) with respect to that of B, following the experimentally observed ratios of B vs R and and G vs R (**Figure S4A**). The simulation shows clearly that this single change in the model parameter does not reproduce the experimental observed differences in the NF-κB response between clones.

Modulating NF-κB amount and amount of activating complexes. **Figure 4G** shows that a variation of the activating complexes can lead to a variation in the response predicted by the model, as observed experimentally (Cruz et al., 2021) (inset of **Figure 4G**). **Figure S4H** shows simulations of the change in the response (taking as reference value clone R) for different changes in the amount of activating complexes (C) and the amount of NF-κB in the model (N_0). This allows us to identify the FC variation in the number of activating complexes and in the amount of NF-κB of B respect to R and of G respect to R that reproduce the observed changes in the NF-κB response upon TNF-α and IL-1β . We repeated the operation using different randomizations of the parameters of R, and then using Matlab optimization tools to find the FC variation of the number of activating complexes C that matched the experimentally observed differences in the response to stimuli between clones (examples of fitting results for different randomizations are shown in **Figure S4I**). The result is shown in **Figure 4H** for TNF-α and in **Figure 5E** for IL-1β

Modulating the amount of NF-κB, activating complexes and Nfkbia transcription. We also model the effect of the variation in the main negative feedback of the system between clones by modulating its transcription rate k. Hence we calculate the variation on k together with the parameters C and N_0, so that the differences in the NF-κB response and in *NFkbia* expression between clone B and R are reproduced for all the random parameter combinations considered, using again Matlab optimization tools. **Figure 6C** shows that the fitting ok k reproduces the experimental ratio of the expression between clones. The resulting changes in the AUC are shown in **Figure 6E**, matching again the differences in AUC observed in the experiments. **Figure 6F** shows instead the effect in the number of peaks, and for 50% of our "oscillatory simulations" (determined by the number of peaks greater or equal than 2) oscillatory peaks are lost.

Mimicking the effect of the ASOs in NF-κB dynamics. To simulate this, we perform different randomization of the parameters of the model for R and then vary the expression of *Nfkbia*, the only parameter affected by ASOs, by fitting properly the transcription rate k. The effect (fold change in the AUC) is then evaluated and found to match the experimentally observed one for most of the parameters (**Figure 6J**).

Downmodulation of IκBa using antisense oligonucleotides. The antisense oligos to target the *Nfkbia* gene were designed by Aum Biotech, LLC (Philadelphia, PA, USA). Four custom antisense oligos in the final concentration of 5 μM were used to treat MEFs for 24 hours to reduce the expression of IκBα.

DATA AND CODE AVAILABILITY

Data on NF-κB dynamics for single cells allowing to reproduce the analysis Figures 1, 2, and 5 are provided in the Source Data file. Gene expression level for the conditions and biological replicates described in Figure 3, 4 and 5 are provided in excel format in the Source Data file.
Bioinformatics analysis tools are available as described in previous section.
Imaging routines to extract NF-κB signaling dynamics in single cells from time lapse movies and mathematical modeling-related code (transcriptomic-constrained estimations of number of complexes and signaling dynamics) can be downloaded at https://github.com/SZambranoS/

SUPPLEMENTARY MATERIAL

Tables:

Table 1: Percentages of cells in each cell cycle phase for each cell population.

	G1 mean intensity	G2 mean intensity	%G1	%G2	%S	G2/G1
Pool	94860,60	180371,15	52,76	14,60	32,65	1,90
Clone B	87175,78	167031,93	43,39	15,82	40,79	1,92
Clone R	97138,36	181729,34	50,84	23,79	25,37	1,87
Clone G	81811,96	153517,46	41,06	18,62	40,32	1,88

Table 2: Length of the genome covered for different coverage thresholds (in bp) using RNA-seq reads, and number of different SNPs identified between clones.

coverage\length	genome covered R	genome covered B	genome covered G	Diff. B vs G	Diff. B vs R	Diff. G vs B
5x	560805040	614001397	576431940	351	301	338
10x	470022271	513879107	480558887	193	172	179
20x	384083108	425738181	392300809	163	108	135

Table 3: Parameters of the mathematical model

These are the starting parameters considered in all our simulations. Each randomization is assumed to described clones R, then only certain parameters are modulated to match experimental observations

and see if they match certain NF-κB dynamic feature. Starting number of NF-κB molecules for clone R is estimated as $3 \cdot 10^3$.

Parameter(s)	Value	units
k_a	$1.9 \cdot 10^{-6}$	molecules^{-1} s^{-1}
k_d	$8.4 \cdot 10^{-6}$	s^{-1}
d_C	$1.3 \cdot 10^{-5}$	s^{-1}
d_K	$2.5 \cdot 10^{-9}$	molecules^{-1} s^{-1}
k_I	$2.5 \cdot 10^{-1}$	s^{-1}
d_I	$6.7 \cdot 10^{-5}$	s^{-1}
k_0	21	molecules^{-1} s^{-1}
d_K	$2.1 \cdot 10^{-4}$	s^{-1}
A_0	$3 \cdot 10^4$	molecules
n	1	-
$k_{t,A}$	$2.5 \cdot 10^{-1}$	s^{-1}
d_A	$6.7 \cdot 10^{-5}$	s^{-1}
k_{on}, $k_{on,A}$	$6.9 \cdot 10^{-8}$	molecules^{-1} s^{-1}
k_{off} , $k_{off,A}$	$4.2 \cdot 10^{-4}$	s^{-1}
δ , δ_A	$7.5 \cdot 10^{-4}$	s^{-1}
k_A, k	$2 \cdot 10^{-1}$	molecules$\cdot$s^{-1}

Supplementary movies:

Movie S1: Dynamics of the pool of MEFs upon 10 ng/ml TNF-α.

Movies S2-S4. Dynamics of clones B, R and G upon 10 ng/ml TNF-α.

Movies S5-S6. Dynamics of clones B and G upon 100 ng/ml IL-1β.

Movies S7-S8. Dynamics of clones treated with mock and *IκBa* targeted ASOs and 10 ng/ml TNF-α.

Supplementary figure captions:

Figure S1. A. Example of nuclei detected using our custom-made software for cell segmentation and tracking. **B.** A realization of our k-means clustering strategy (k=9), where NF-κB dynamic profiles of cells from the 8 clonal populations and the pool are clustered according to their shape in 9 clusters. **C.** Example of the histogram with the number of cells of each population observed in each cluster generated in S1B. **D.** Example of the computed probability of co-clustering of NF-κB dynamic profiles of each population in a given cluster in a single realization of the stochastic clustering algorithm.

Figure S2. A. Dynamic heatmap of the response of the clones B, R and G to 10 ng/ml TNF-α in biological triplicates. **B.** Average NF-κB dynamic profiles of pool and the three clones upon 100 ng/ml TNF-α. **C.** Average NF-κB dynamic profiles of the pool and the three clones B, R, G kept in culture for 8 weeks. **D.** Coefficient of variation (standard deviation divided by the mean) of the pool and the three clones. **E.** Dynamical features of the response to TNF-α in three biological replicates: value of the first peak, timing and area under the curve (AUC). **F.** Average basal initial NCI value (before stimulation) for the three clones. **G.** Features of NF-κB dynamics of the pool and three clones quantified by absolute NF-κB intensities. **H.** Maximum response to TNF-α computed by manually segmenting the nuclei. **I.** Estimation of the cell cycle phases of each population by FACS analysis. **J.** Values of the AUC obtained for clone B, clone R, and clone R by correcting in silico for the differences in cell cycle between B and R. **K.** Distribution of the number of peaks in the three clones for 8 hours of TNF-α stimulation. **L.** Ratios of the peak values for different peak numbers calculated in three experimental replicates per population, *$p<10^{-2}$, ** $p<10^{-3}$, *** $p<10^{-4}$, multiple comparisons through Kruskal-Wallis.

Figure S3. A. Density plot of normalized expressed genes for each sample. **B.** Estimated frequency of substitution between clones calculated by the ratio of the number of SNPs and the length of the mapped genome. Increasing marker sizes indicate more stringent criteria for SNPs calling (5x, 10x and 20x coverage). **C.** Additional dimensions of the PCA for our samples' transcriptomes and fraction of variance explained. **D.** PCA of samples from our clones performed jointly with transcriptomic data from two other mouse tissues. **E.** Hierarchical clustering of the genes from the "TNF-α NF-κB signaling pathway (Mus musculus)" list from *Wikipathways*. **F.** Additional dimensions of the PCA when considering only NF-κB targets and fraction of variance explained per dimension. **G.** Volcano plot for the transcriptomic data of the pool. **H.** KEGG enriched pathways when looking at genes up/down regulated upon TNF-α in the indicated clones.

Figure S4. A. Expression of RelA gene assessed by RNA-seq plotted against the average fluorescent intensity of the protein per cell in each clonal population with respect to clone R. Error bars denote standard deviation of each measurement, dashed line represents perfect identity. **B.** Fold change expression of genes in the "TNF-α to NF-κB" list, B vs R against G vs R values. **C.** ssGSEA analysis of the "TNF-α to NF-κB" samples (multiple comparisons, Kruskal-Wallis). **D.** Examples of simulations of

association-dissociation reaction dynamics for different values of the dissociation constant (K_D); circles indicate equilibria inferred from the equilibrium equations. **E.** Transcriptomic-constrained prediction of the FC in the number of complexes formed upon TNF-α for clone B vs R, and for G vs R, for different values of Δ and K_D. **F.** Variability in our transcriptomic-constrained prediction of the simulations of E., computed as the standard deviation of the simulations. **G.** Numerical simulation with our mathematical model of NF-κB dynamics of the clone R (red line) and varying only the NF-κB amount to mimic the experimentally observed higher values of clone B and G (dashed blue and green, respectively). **H.** Numerical simulation of the variation in the NF-κB response with NF-κB amount and with the number of activating complexes using our mathematical model. Dashed color lines lines indicate experimentally observed levels of NF-κB for clone B and G, taken R as reference. Crosses indicate combinations reproducing the experimentally observed variation B vs R and G vs R for TNF-α, displayed on the colorbar with gray dashed lines. Circles indicate the same, but for IL-1β. **I.** Examples of randomizations where we have reproduced the procedure schematically represented in H, so the differences in the response (first peak NCI) match those observed experimentally (on average).

Figure S5. A. Fold change expression of genes in the "IL-1β to NF-κB" list, B vs R against G vs R values. **B.** ssGSEA analysis of the "IL-1β to NF-κB", only samples from B show statistical difference with the rest. **C.** Transcriptomic-constrained prediction of the number of complexes formed upon IL-1β for clone B vs R, and for G vs R, for different values of Δ and maximum values of K_D considered. **D.** Variability in our transcriptomic-constrained prediction shown in C., computed as the standard deviations of the simulations performed for each pair of K_D considered and Δ. **E.** Dynamical features of the response to IL-1β in two biological replicates. **F.** Features of the oscillatory peaks across the populations of clones upon IL-1β. *$p<10^{-2}$, ** $p<10^{-3}$,*** $p<10^{-4}$, multiple comparisons through Kruskal-Wallis.

Figure S6. A. Numerical simulation for the parameter set of Table 3 of the variation in the AUC of the NF-κB dynamics with the NF-κB amount and the number of activating complexes. Dashed lines indicate experimentally observed levels of NF-κB for clone B and G, taken R as reference. Crosses indicate combinations reproducing the early NF-κB responses observed for TNF-α, circles for IL-1β. **B.** Fold change expression levels of IκBα by RT-qPCR. Error bars show the standard deviation of replicates. **C.** Relative expression of the other negative feedbacks with respect to the Nfkbia expression for R. **D.** Representative images in the Hoechst channel show internalization of the ASOs after 24 hours. **E.** Relative mRNA levels of IκBα after 24 hours of ASO treatment. Error bars show the standard deviation of replicates. **F.** Effect of the scrambled (MOCK) ASOs and ASOs targeting IκBα on the maximum and AUC of the pool population. **G.** Quantification of the maximum response and **H.** the AUC for untreated and ASO-treated cells upon TNF-α in a biological replicate of the experiment shown in Figure 6. *$p<10^{-2}$, ** $p<10^{-3}$,*** $p<10^{-4}$, multiple comparisons through Kruskal-Wallis except in panel C, where two-way Anova was used.

REFERENCES

Adelaja A, Taylor B, Sheu KM, Liu Y, Luecke S, Hoffmann A. 2021. Six distinct NFκB signaling codons convey discrete information to distinguish stimuli and enable appropriate macrophage responses. *Immunity* **54**:916-930.e7. doi:10.1016/j.immuni.2021.04.011

Adetunji MO, Lamont SJ, Abasht B, Schmidt CJ. 2019. Variant analysis pipeline for accurate detection of genomic variants from transcriptome sequencing data. *PLoS One* **14**:e0216838. doi:10.1371/journal.pone.0216838

A.Hoffmann, Levchencko A, Scott ML, Baltimore D. 2002. The IkappaB-NF-kappaB signalling module: temporal control and selective gene activation. *Science* **298**:1241–1245.

Alon U. 2007. An Introduction to Systems Biology. Boca Raton, FL (USA): CRC Press.

Amand MM, Hanover JA, Shiloach J. 2016. A comparison of strategies for immortalizing mouse embryonic fibroblasts. *Journal of Biological Methods* **3**:e41–e41. doi:10.14440/jbm.2016.110

Ankers JM, Awais R, Jones NA, Boyd J, Ryan S, Adamson AD, Harper CV, Bridge L, Spiller DG, Jackson DA, Paszek P, Sée V, White MR. 2016. Dynamic NF-κB and E2F interactions control the priority and timing of inflammatory signalling and cell proliferation. *eLife* **5**:e10473. doi:10.7554/eLife.10473

Ashall L, Horton CA, Nelson DE, Paszek P, Harper CV, Sillitoe K, Ryan S, Spiller DG, Unitt JF, Broomhead DS, Kell DB, Rand DA, See V, White MRH. 2009. Pulsatile Stimulation Determines Timing and Specificity of NF- B-Dependent Transcription. *Science* **324**:242–246. doi:10.1126/science.1164860

Barbie DA, Tamayo P, Boehm JS, Kim SY, Moody SE, Dunn IF, Schinzel AC, Sandy P, Meylan E, Scholl C, Fröhling S, Chan EM, Sos ML, Michel K, Mermel C, Silver SJ, Weir BA, Reiling JH, Sheng Q, Gupta PB, Wadlow RC, Le H, Hoersch S, Wittner BS, Ramaswamy S, Livingston DM, Sabatini DM, Meyerson M, Thomas RK, Lander ES, Mesirov JP, Root DE, Gilliland DG, Jacks T, Hahn WC. 2009. Systematic RNA interference reveals that oncogenic KRAS-driven cancers require TBK1. *Nature* **462**:108–112. doi:10.1038/nature08460

Barken D, Wang CJ, Kearns J, Cheong R, Hoffmann A, Levchenko A. 2005. Comment on "Oscillations in NF-κB Signaling Control the Dynamics of Gene Expression." *Science* **308**:52–52. doi:10.1126/science.1107904

Beg AA, Baltimore D. 1996. An Essential Role for NF-κB in Preventing TNF-α-Induced Cell Death. *Science* **274**:782–784. doi:10.1126/science.274.5288.782

Brambilla F, Garcia-Manteiga JM, Monteleone E, Hoelzen L, Zocchi A, Agresti A, Bianchi ME. 2020. Nucleosomes effectively shield DNA from radiation damage in living cells. *Nucleic Acids Research* **48**:8993–9006. doi:10.1093/nar/gkaa613

Careccia G Colombo, F, Tirone, M, Agresti,A, Bianchi, ME, Zambrano, S, Vénéreau, E. 2019. Exploiting Live Imaging to Track Nuclei During Myoblast Differentiation and Fusion. *Journal of visualized experiments : JoVE* **In press**.

Cheng QJ, Ohta S, Sheu KM, Spreafico R, Adelaja A, Taylor B, Hoffmann A. 2021. NF-κB dynamics determine the stimulus specificity of epigenomic reprogramming in macrophages. *Science* **372**:1349–1353. doi:10.1126/science.abc0269

Cruz JA, Mokashi CS, Kowalczyk GJ, Guo Y, Zhang Q, Gupta S, Schipper DL, Smeal SW, Lee REC. 2021. A variable-gain stochastic pooling motif mediates information transfer from receptor assemblies into NF-κB. *Sci Adv* **7**:eabi9410. doi:10.1126/sciadv.abi9410

De Lorenzi R, Gareus R, Fengler S, Pasparakis M. 2009. GFP-p65 knock-in mice as a tool to study NF-κB dynamics in vivo. *genesis* **47**:323–329. doi:10.1002/dvg.20468

DeFelice MM, Clark HR, Hughey JJ, Maayan I, Kudo T, Gutschow MV, Covert MW, Regot S. 2019. NF-κB signaling dynamics is controlled by a dose-sensing autoregulatory loop. *Sci Signal* **12**. doi:10.1126/scisignal.aau3568

Ferrell JE, Tsai TY-C, Yang Q. 2011. Modeling the Cell Cycle: Why Do Certain Circuits Oscillate? *Cell* **144**:874–885. doi:10.1016/j.cell.2011.03.006

Franklin JM, Ghosh RP, Shi Q, Reddick MP, Liphardt JT. 2020. Concerted localization-resets precede YAP-dependent transcription. *Nat Commun* **11**:4581. doi:10.1038/s41467-020-18368-x

Gapuzan M-ER, Schmah O, Pollock AD, Hoffmann A, Gilmore TD. 2005. Immortalized fibroblasts from NF-kappaB RelA knockout mice show phenotypic heterogeneity and maintain increased sensitivity to tumor necrosis factor alpha after transformation by v-Ras. *Oncogene* **24**:6574–6583. doi:10.1038/sj.onc.1208809

Greaves M, Maley CC. 2012. CLONAL EVOLUTION IN CANCER. *Nature* **481**:306–313. doi:10.1038/nature10762

Hayden MS, Ghosh S. 2008. Shared Principles in NF-kappaB Signaling. *Cell* **132**:344–344.

Hoffmann A, Levchencko A, Scott ML, Baltimore D. 2002. The IkappaB-NF-kappaB signalling module: temporal control and selective gene activation. *Science* **298**:1241–1245.

Hsu H, Shu H-B, Pan M-G, Goeddel DV. 1996. TRADD–TRAF2 and TRADD–FADD Interactions Define Two Distinct TNF Receptor 1 Signal Transduction Pathways. *Cell* **84**:299–308. doi:10.1016/S0092-8674(00)80984-8

Hwang B, Phan FP, McCool K, Choi EY, You J, Johnson A, Audhya A, Miyamoto S. 2015. Quantification of Cellular NEMO Content and Its Impact on NF-κB Activation by Genotoxic Stress. *PLOS ONE* **10**:e0116374. doi:10.1371/journal.pone.0116374

Kellogg R, Tay S. 2015. Noise facilitates transcriptional control under dynamic inputs. *Cell* **160**:381–392.

Kizilirmak C, Bianchi ME, Zambrano S. 2022. Insights on the NF-κB System Using Live Cell Imaging: Recent Developments and Future Perspectives. *Frontiers in Immunology* **13**.

Kull T, Wehling A, Etzrodt M, Auler M, Dettinger P, Aceto N, Schroeder T. 2022. NfκB signaling dynamics and their target genes differ between mouse blood cell types and induce distinct cell behavior. *Blood* **140**:99–111. doi:10.1182/blood.2021012918

Lane K, Van Valen D, DeFelice MM, Macklin DN, Kudo T, Jaimovich A, Carr A, Meyer T, Pe'er D, Boutet SC, Covert MW. 2017. Measuring Signaling and RNA-Seq in the Same Cell Links Gene Expression to Dynamic Patterns of NF-κB Activation. *Cell Syst* **4**:458-469.e5. doi:10.1016/j.cels.2017.03.010

Lee RE, Walker SR, Savery K, Frank DA, Gaudet S. 2014. Fold change of nuclear NF-kappaB determines TNF-induced transcription in single cells. *Mol Cell* **53**:867–879.

Lee REC, Qasaimeh MA, Xia X, Juncker D, Gaudet S. 2016. NF-κB signalling and cell fate decisions in response to a short pulse of tumour necrosis factor. *Scientific Reports* **6**:39519. doi:10.1038/srep39519

Lee TK, Denny EM, Sanghvi JC, Gaston JE, Maynard ND, Hughey JJ, Covert MW. 2009. A Noisy Paracrine Signal Determines the Cellular NF-kappaB response to Lipopolysaccharide. *Science Signalling* **2**:1–9.

Levine JH, Lin Y, Elowitz MB. 2013. Functional Roles of Pulsing in Genetic Circuits. *Science* **342**:1193–1193.

Li Y, Shan Y, Desai RV, Cox KH, Weinberger LS, Takahashi JS. 2020. Noise-driven cellular heterogeneity in circadian periodicity. *PNAS* **117**:10350–10356. doi:10.1073/pnas.1922388117

Lynch MD, Watt FM. 2018. Fibroblast heterogeneity: implications for human disease. *J Clin Invest* **128**:26–35. doi:10.1172/JCI93555

Martin EW, Pacholewska A, Patel H, Dashora H, Sung M-H. 2020. Integrative analysis suggests cell type–specific decoding of NF-κB dynamics. *Sci Signal* **13**. doi:10.1126/scisignal.aax7195

Martin MU, Wesche H. 2002. Summary and comparison of the signaling mechanisms of the Toll/interleukin-1 receptor family. *Biochimica et Biophysica Acta (BBA) - Molecular Cell Research*, The Molecular Biology of Cytokines **1592**:265–280. doi:10.1016/S0167-4889(02)00320-8

Matsuda M, Hayashi H, Garcia-Ojalvo J, Yoshioka-Kobayashi K, Kageyama R, Yamanaka Y, Ikeya M,

Toguchida J, Alev C, Ebisuya M. 2020. Species-specific segmentation clock periods are due to differential biochemical reaction speeds. *Science* **369**:1450–1455. doi:10.1126/science.aba7668

Milholland B, Dong X, Zhang L, Hao X, Suh Y, Vijg J. 2017. Differences between germline and somatic mutation rates in humans and mice. *Nat Commun* **8**:15183. doi:10.1038/ncomms15183

Milo R, Phillips R. 2015. Cell Biology by the Numbers. CRC Press.

Natoli G, Ostuni R. 2019. Adaptation and memory in immune responses. *Nat Immunol* **20**:783–792. doi:10.1038/s41590-019-0399-9

Nelson DE, Horton CA, See V, Johnson JR, Nelson G, Spiller DG, Kell DB, White MRH. 2005. Response to Comment on "Oscillations in NF-κB Signaling Control the Dynamics of Gene Expression." *Science* **308**:52–52. doi:10.1126/science.1108198

Nelson DE, Ihekwaba AE, Elliott M, Johnson JR, Gibney CA, Foreman BE, Nelson G, See V, Horton CA, Spiller DG, Edwards SW, McDowell HP, Unitt JF, Sullivan E, Grimley R, Benson N, Broomhead D, Kell DB, White MR. 2004. Oscillations in NF-kappaB signaling control the dynamics of gene expression. *Science* **306**:704–708.

Paek AL, Liu JC, Loewer A, Forrester WC, Lahav G. 2016. Cell-to-Cell Variation in p53 Dynamics Leads to Fractional Killing. *Cell* **165**:631–642. doi:10.1016/j.cell.2016.03.025

Paszek P, Ryan S, Ashall L, Sillitoe K, Harper CV, Spiller DG, Rand DA, White MRH. 2010. Population robustness arising from cellular heterogeneity. *Proc Natl Acad Sci USA* **107**:11644–11649.

Patke A, Young MW, Axelrod S. 2020. Molecular mechanisms and physiological importance of circadian rhythms. *Nat Rev Mol Cell Biol* **21**:67–84. doi:10.1038/s41580-019-0179-2

Purvis JE, Lahav G. 2013. Encoding and decoding cellular information through signaling dynamics. *Cell* **152**:945–956. doi:10.1016/j.cell.2013.02.005

Purvis JE, Mock KWKC, Batchelor E, Loewer A, Lahav G. 2012. p53 Dynamics Control Cell Fate. *Science* **336**:1440–1444.

Rahman SMT, Aqdas M, Martin EW, Ardori FT, Songkiatisak P, Oh K-S, Uderhardt S, Yun S, Claybourne QC, McDevitt RA, Greco V, Germain RN, Tessarollo L, Sung M-H. 2022. Double knockin mice show NF-κB trajectories in immune signaling and aging. *Cell Reports* **41**. doi:10.1016/j.celrep.2022.111682

Rhyasen GW, Starczynowski DT. 2015. IRAK signalling in cancer. *Br J Cancer* **112**:232–237. doi:10.1038/bjc.2014.513

Schmitz ML, Baeuerle PA. 1991. The p65 subunit is responsible for the strong transcription activating potential of NF-kappa B. *The EMBO journal* **10**:3805–17.

Selimkhanov J, Taylor B, Yao J, Pilko A, Albeck J, Hoffmann A, Tsimring L, Wollman R. 2014. Accurate information transmission through dynamic biochemical signaling networks. *Science* **346**:1370–1373. doi:10.1126/SCIENCE.1254933

Sen S, Cheng Z, Sheu KM, Chen YH, Hoffmann A. 2020. Gene Regulatory Strategies that Decode the Duration of NFκB Dynamics Contribute to LPS- versus TNF-Specific Gene Expression. *Cell Syst* **10**:169-182.e5. doi:10.1016/j.cels.2019.12.004

Son M, Wang AG, Tu H-L, Metzig MO, Patel P, Husain K, Lin J, Murugan A, Hoffmann A, Tay S. 2021. NF-κB responds to absolute differences in cytokine concentrations. *Sci Signal* **14**. doi:10.1126/scisignal.aaz4382

Su CJ, Murugan A, Linton JM, Yeluri A, Bois J, Klumpe H, Langley MA, Antebi YE, Elowitz MB. 2022. Ligand-receptor promiscuity enables cellular addressing. *cels* **13**:408-425.e12. doi:10.1016/j.cels.2022.03.001

Sung M-H, Li N, Lao Q, Gottschalk RA, Hager GL, Fraser IDC. 2014. Switching of the Relative Dominance Between Feedback Mechanisms in Lipopolysaccharide-Induced NF-κB Signaling. *Sci Signal* **7**:ra6–ra6. doi:10.1126/scisignal.2004764

Sung MH, Salvatore L, Lorenzi RD, Indrawan A, Pasparakis M, Hager GL, Bianchi ME, Agresti A. 2009.

Sustained Oscillations of NF-kappaB Produce Distinct Genome Scanning and Gene Expression Profiles. *PLoS ONE* **5**:e7163–e7163.

Tay S, Hughey JJ, Lee TK, Lipniacki T, Quake SR, Covert MW. 2010. Single-cell NF-kappaB dynamics reveal digital activation and analogue information processing. *Nature* **466**:267–271.

Todaro GJ, Green H. 1963. QUANTITATIVE STUDIES OF THE GROWTH OF MOUSE EMBRYO CELLS IN CULTURE AND THEIR DEVELOPMENT INTO ESTABLISHED LINES. *J Cell Biol* **17**:299–313.

Wilson NS, Dixit V, Ashkenazi A. 2009. Death receptor signal transducers: nodes of coordination in immune signaling networks. *Nat Immunol* **10**:348–355. doi:10.1038/ni.1714

Zambrano S, Bianchi ME, Agresti A. 2014a. High-throughput analysis of NF-κB dynamics in single cells reveals basal nuclear localization of NF-κB and spontaneous activation of oscillations. *PLoS ONE* **9**. doi:10.1371/journal.pone.0090104

Zambrano S, Bianchi ME, Agresti A. 2014b. A simple model of NF-κB dynamics reproduces experimental observations. *Journal of Theoretical Biology* **347**. doi:10.1016/j.jtbi.2014.01.015

Zambrano S, de Toma I, Piffer A, Bianchi ME, Agresti A. 2016. NF-kappaB oscillations translate into functionally related patterns of gene expression. *eLife* **5**:e09100–e09100.

Zambrano S, Loffreda A, Carelli E, Stefanelli G, Colombo F, Bertrand E, Tacchetti C, Agresti A, Bianchi ME, Molina N, Mazza D. 2020. First Responders Shape a Prompt and Sharp NF-κB-Mediated Transcriptional Response to TNF-α. *iScience* **23**:101529. doi:10.1016/j.isci.2020.101529

Zhang Q, Gupta S, Schipper DL, Kowalczyk GJ, Mancini AE, Faeder JR, Lee REC. 2017. NF-κB dynamics discriminate between TNF doses in single cells. *Cell Syst* **5**:638-645.e5. doi:10.1016/j.cels.2017.10.011

Zhang Z-B, Wang Q-Y, Ke Y-X, Liu S-Y, Ju J-Q, Lim WA, Tang C, Wei P. 2017. Design of Tunable Oscillatory Dynamics in a Synthetic NF-κB Signaling Circuit. *Cell Systems* **5**:460-470.e5. doi:10.1016/J.CELS.2017.09.016

Figure 1

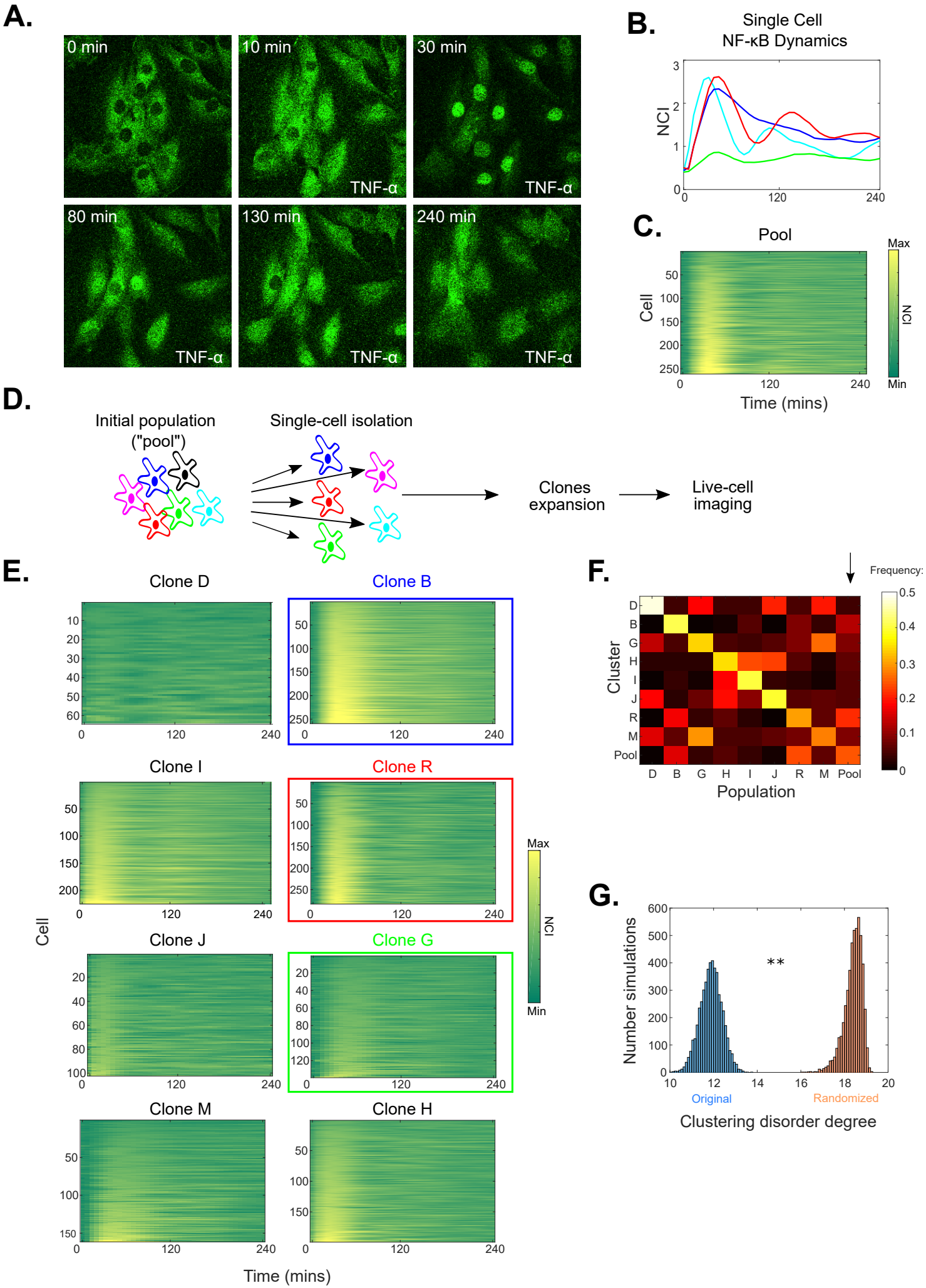
A.
0 min
10 min
30 min
80 min
130 min
240 min
TNF-α
B.
Single Cell
NF-κB Dynamics
NCI
C.
Pool
Cell
Max
Min
Time (mins)
D.
Initial population
("pool")
Single-cell isolation
Clones
expansion
Live-cell
imaging
E.
Clone D
Clone B
Clone I
Clone R
Clone J
Clone G
Clone M
Clone H
Cell
Time (mins)
F.
Frequency:
Cluster
Population
D B G H I J R M Pool
G.
Number simulations
Original
Randomized
Clustering disorder degree

Figure 2

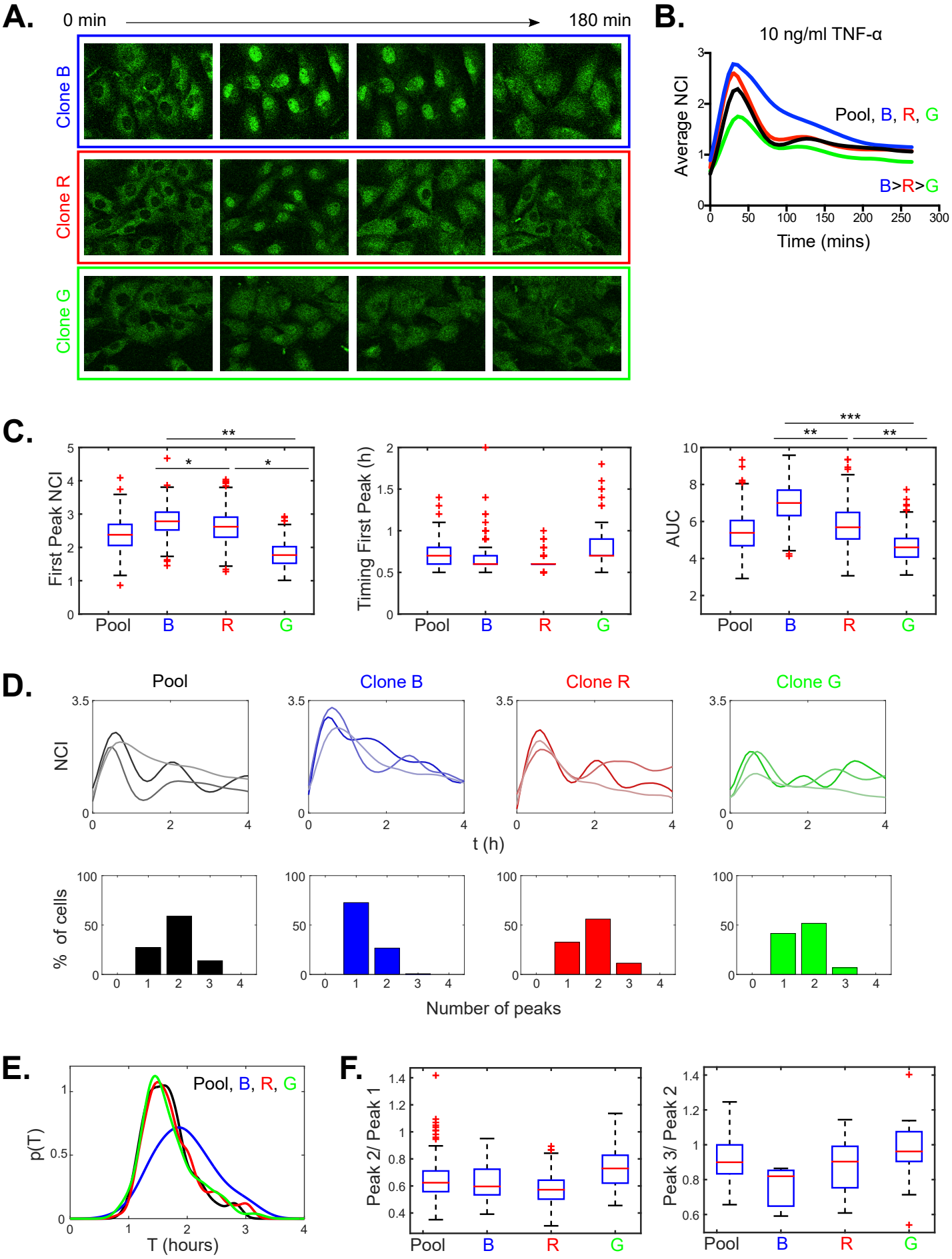
A.
0 min
180 min
Clone B
Clone R
Clone G
B.
10 ng/ml TNF-α
Average NCI
Pool, B, R, G
B>R>G
Time (mins)
C.
First Peak NCI
Timing First Peak (h)
AUC
Pool
B
R
G
D.
Pool
Clone B
Clone R
Clone G
NCI
t (h)
% of cells
Number of peaks
E.
p(T)
Pool, B, R, G
T (hours)
F.
Peak 2/ Peak 1
Peak 3/ Peak 2

Figure 3

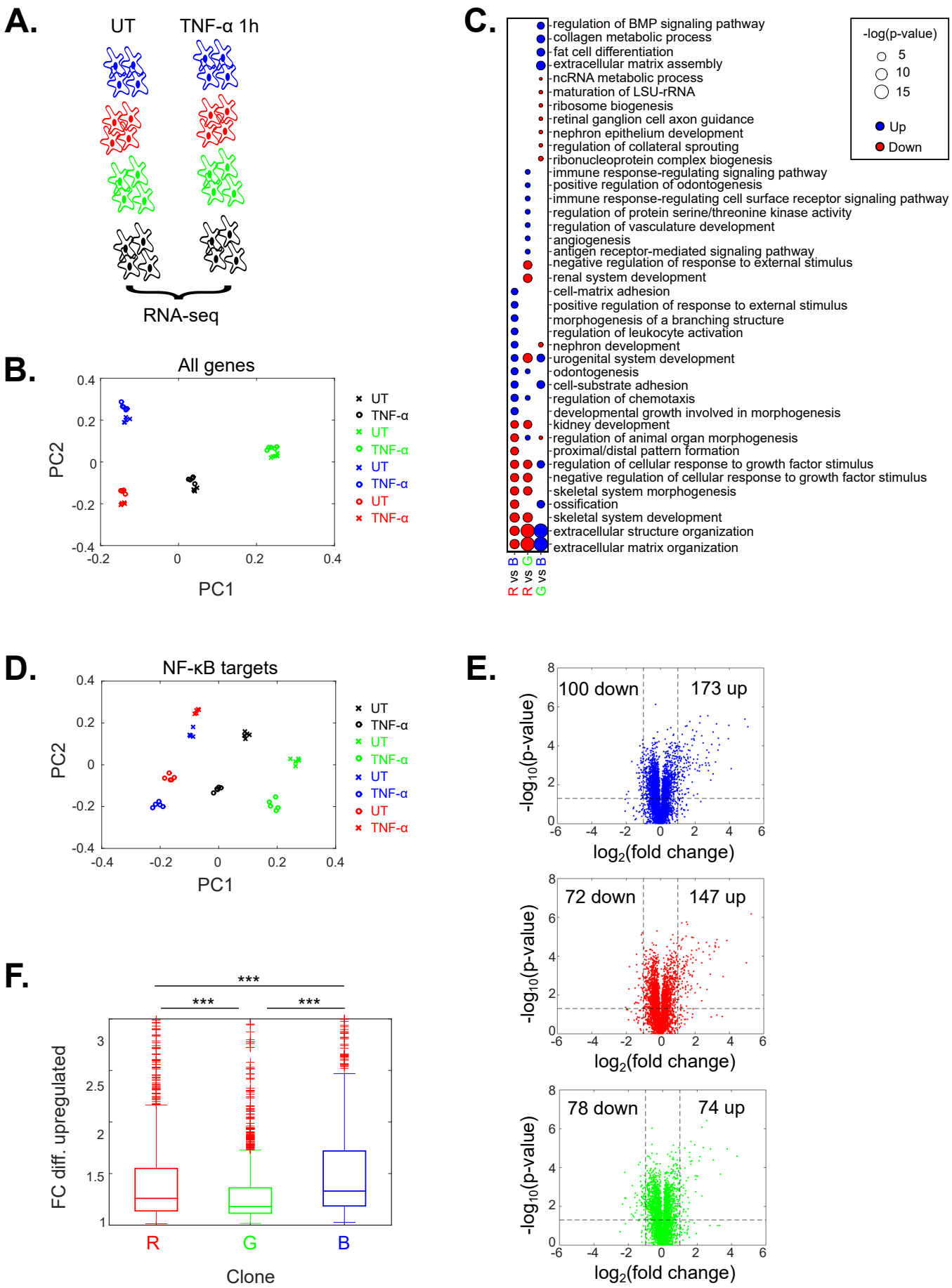
A.
UT
TNF-α 1h
RNA-seq
B.
All genes
PC2
PC1
UT
TNF-α
C.
-log(p-value)
5
10
15
Up
Down
regulation of BMP signaling pathway
collagen metabolic process
fat cell differentiation
extracellular matrix assembly
ncRNA metabolic process
maturation of LSU-rRNA
ribosome biogenesis
retinal ganglion cell axon guidance
nephron epithelium development
regulation of collateral sprouting
ribonucleoprotein complex biogenesis
immune response-regulating signaling pathway
positive regulation of odontogenesis
immune response-regulating cell surface receptor signaling pathway
regulation of protein serine/threonine kinase activity
regulation of vasculature development
angiogenesis
antigen receptor-mediated signaling pathway
negative regulation of response to external stimulus
renal system development
cell-matrix adhesion
positive regulation of response to external stimulus
morphogenesis of a branching structure
regulation of leukocyte activation
nephron development
urogenital system development
odontogenesis
cell-substrate adhesion
regulation of chemotaxis
developmental growth involved in morphogenesis
kidney development
regulation of animal organ morphogenesis
proximal/distal pattern formation
regulation of cellular response to growth factor stimulus
negative regulation of cellular response to growth factor stimulus
skeletal system morphogenesis
ossification
skeletal system development
extracellular structure organization
extracellular matrix organization
R vs B
R vs G
G vs B
D.
NF-κB targets
PC2
PC1
UT
TNF-α
E.
100 down
173 up
72 down
147 up
78 down
74 up
-log10(p-value)
log2(fold change)
F.
***
FC diff. upregulated
R
G
B
Clone

Figure 4

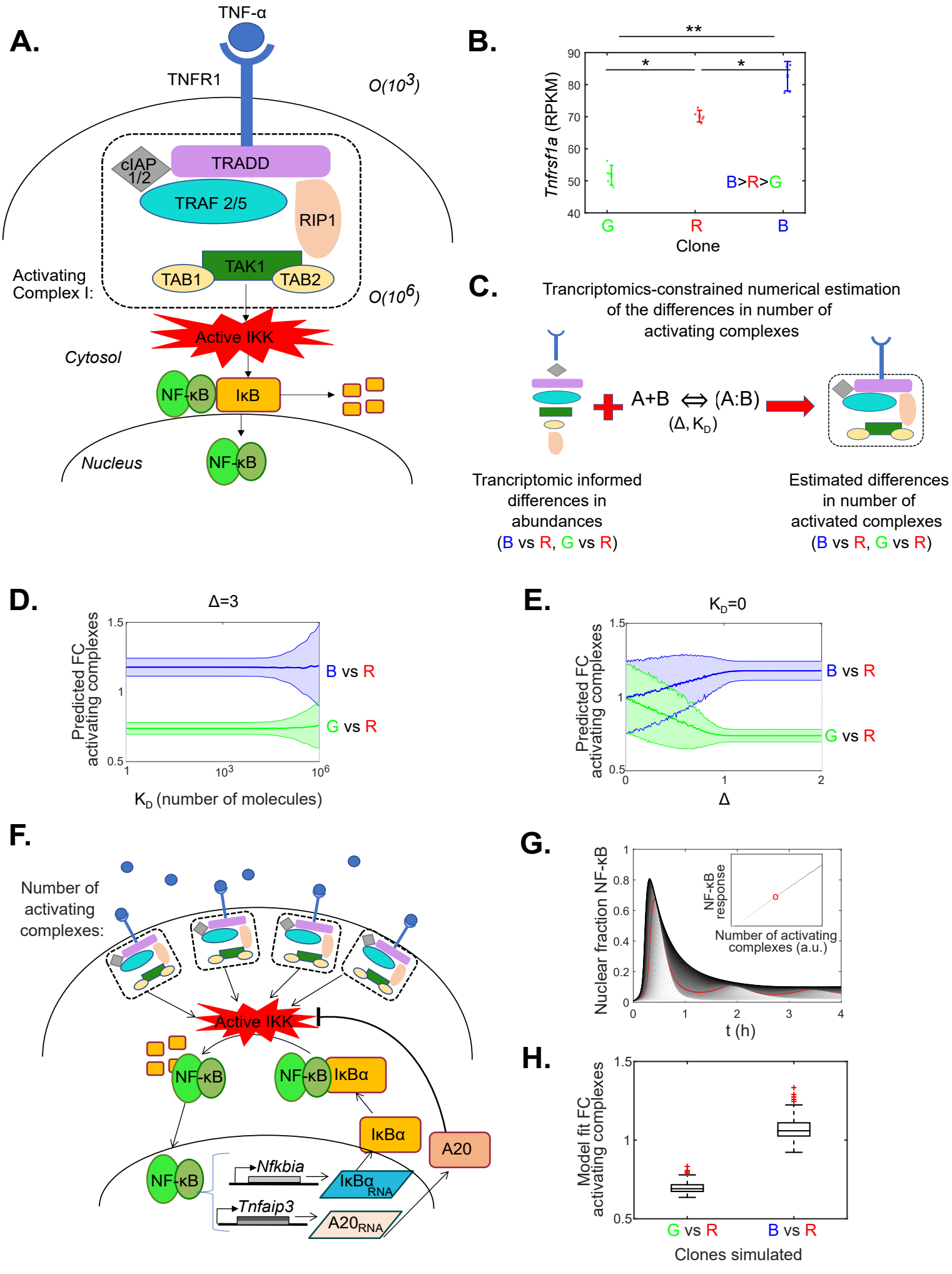
A.
TNF-α
TNFR1
O(10^3)
cIAP 1/2
TRADD
TRAF 2/5
RIP1
TAK1
TAB1
TAB2
Activating Complex I:
O(10^6)
Active IKK
Cytosol
NF-κB
IκB
Nucleus
NF-κB
B.
Tnfrsf1a (RPKM)
B>R>G
G
R
B
Clone
C.
Trancriptomics-constrained numerical estimation of the differences in number of activating complexes
A+B ⇔ (A:B)
(Δ, K_D)
Trancriptomic informed differences in abundances (B vs R, G vs R)
Estimated differences in number of activated complexes (B vs R, G vs R)
D.
Δ=3
Predicted FC activating complexes
B vs R
G vs R
K_D (number of molecules)
E.
K_D=0
Predicted FC activating complexes
B vs R
G vs R
Δ
F.
Number of activating complexes:
Active IKK
NF-κB
NF-κB
IκBα
IκBα
A20
NF-κB
Nfkbia
IκBα RNA
Tnfaip3
A20 RNA
G.
Nuclear fraction NF-κB
NF-κB response
Number of activating complexes (a.u.)
t (h)
H.
Model fit FC activating complexes
G vs R
B vs R
Clones simulated

Figure 5

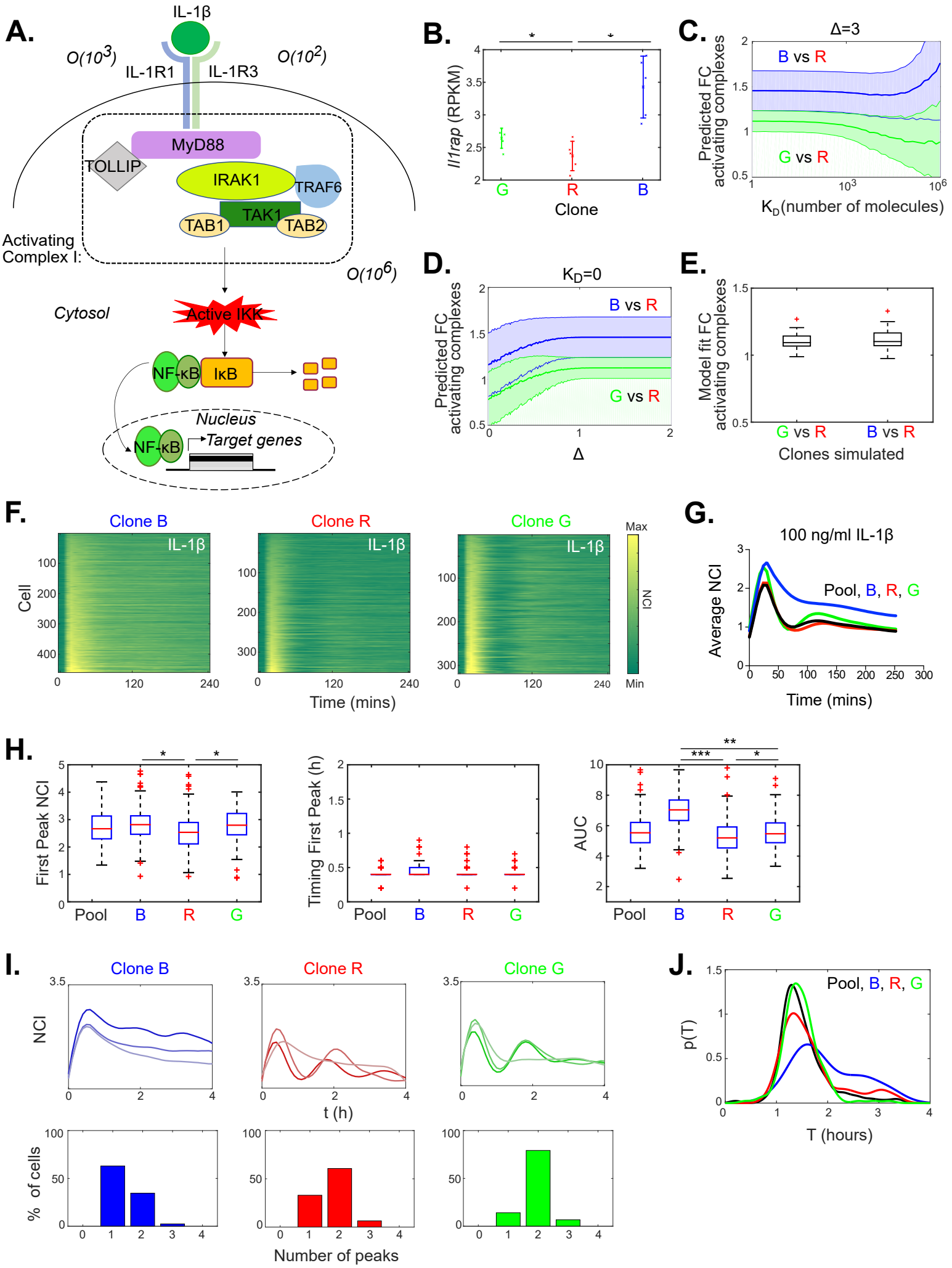
A.
IL-1β
O(10^3)
O(10^2)
IL-1R1
IL-1R3
MyD88
TOLLIP
IRAK1
TRAF6
TAK1
TAB1
TAB2
Activating Complex I:
O(10^6)
Cytosol
Active IKK
NF-κB
IκB
Nucleus
NF-κB
Target genes
B.
Il1rap (RPKM)
G
R
B
Clone
C.
Δ=3
B vs R
G vs R
Predicted FC activating complexes
K_D(number of molecules)
D.
K_D=0
B vs R
G vs R
Predicted FC activating complexes
Δ
E.
Model fit FC activating complexes
G vs R
B vs R
Clones simulated
F.
Clone B
Clone R
Clone G
IL-1β
Cell
Max
Min
NCI
Time (mins)
G.
100 ng/ml IL-1β
Pool, B, R, G
Average NCI
Time (mins)
H.
First Peak NCI
Timing First Peak (h)
AUC
Pool
B
R
G
I.
Clone B
Clone R
Clone G
NCI
t (h)
% of cells
Number of peaks
J.
Pool, B, R, G
p(T)
T (hours)

Figure 6

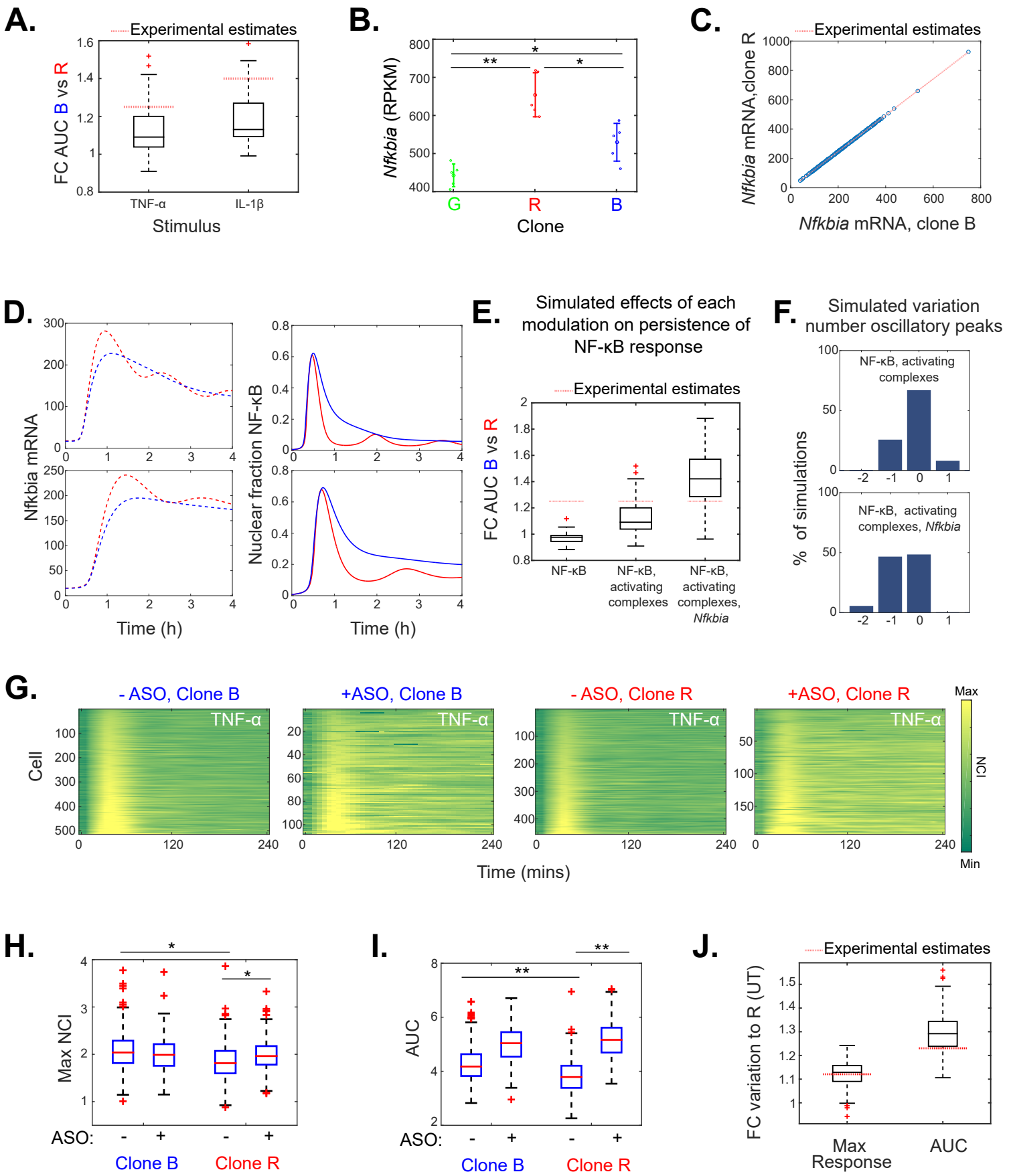
A.
Experimental estimates
FC AUC B vs R
TNF-α
IL-1β
Stimulus
B.
Nfkbia (RPKM)
G
R
B
Clone
C.
Experimental estimates
Nfkbia mRNA,clone R
Nfkbia mRNA, clone B
D.
Nfkbia mRNA
Nuclear fraction NF-κB
Time (h)
E.
Simulated effects of each modulation on persistence of NF-κB response
Experimental estimates
FC AUC B vs R
NF-κB
NF-κB, activating complexes
NF-κB, activating complexes, Nfkbia
F.
Simulated variation number oscillatory peaks
NF-κB, activating complexes
NF-κB, activating complexes, Nfkbia
% of simulations
G.
- ASO, Clone B
+ASO, Clone B
- ASO, Clone R
+ASO, Clone R
TNF-α
Cell
Time (mins)
Max
Min
NCI
H.
Max NCI
ASO:
Clone B
Clone R
I.
AUC
ASO:
Clone B
Clone R
J.
Experimental estimates
FC variation to R (UT)
Max Response
AUC

Supp. Figure S1

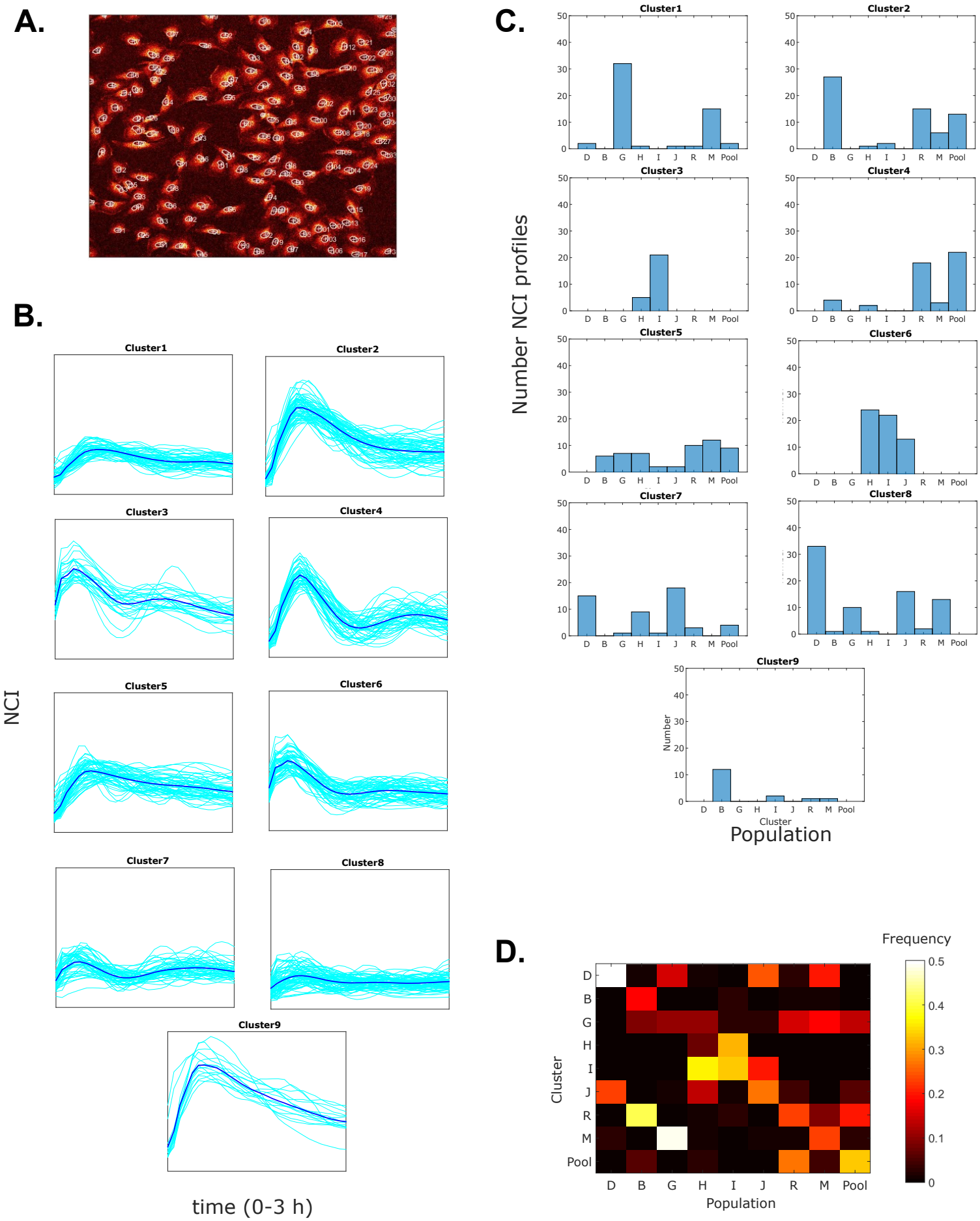

Supp. Figure S2

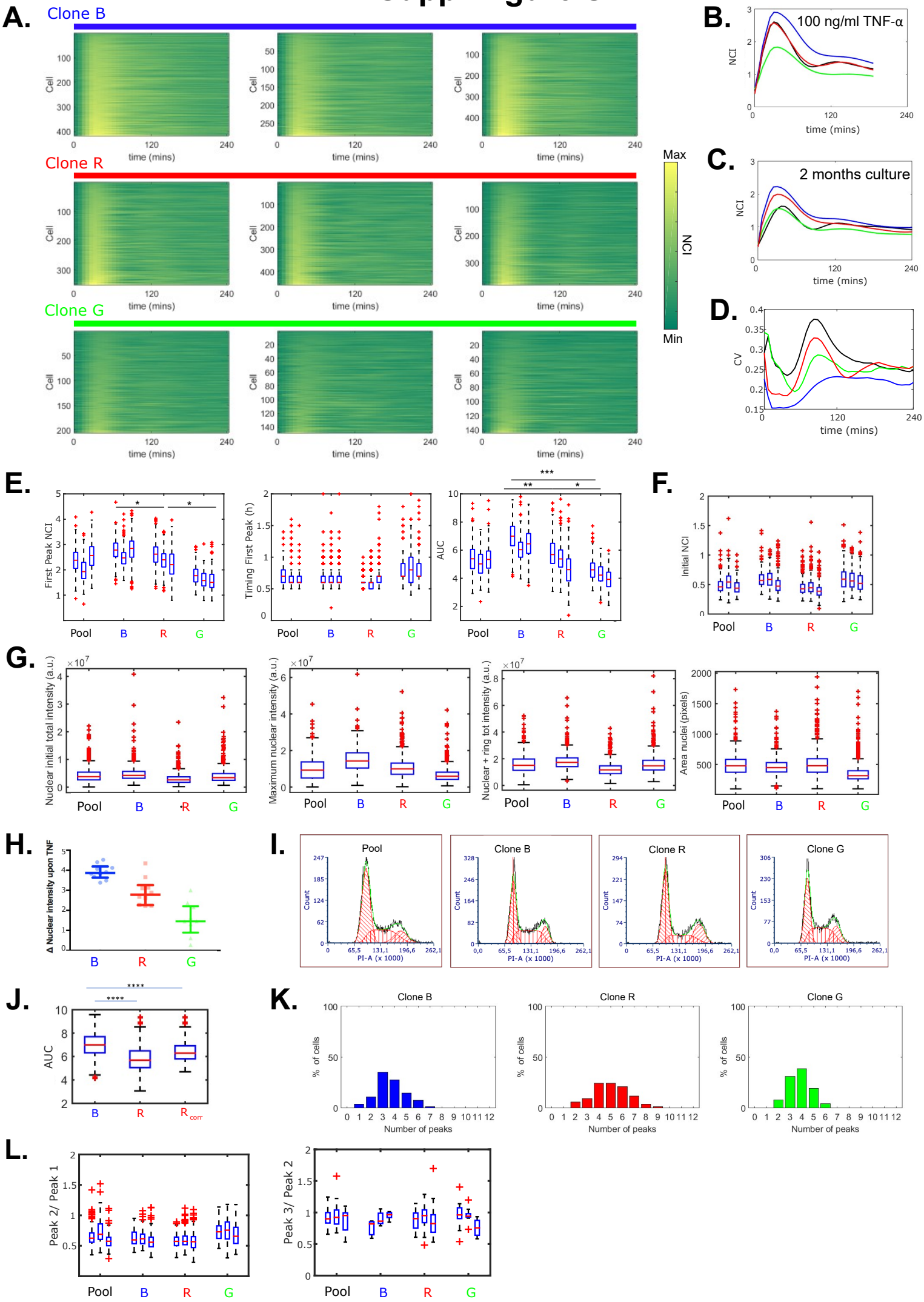

Supp. Figure S3

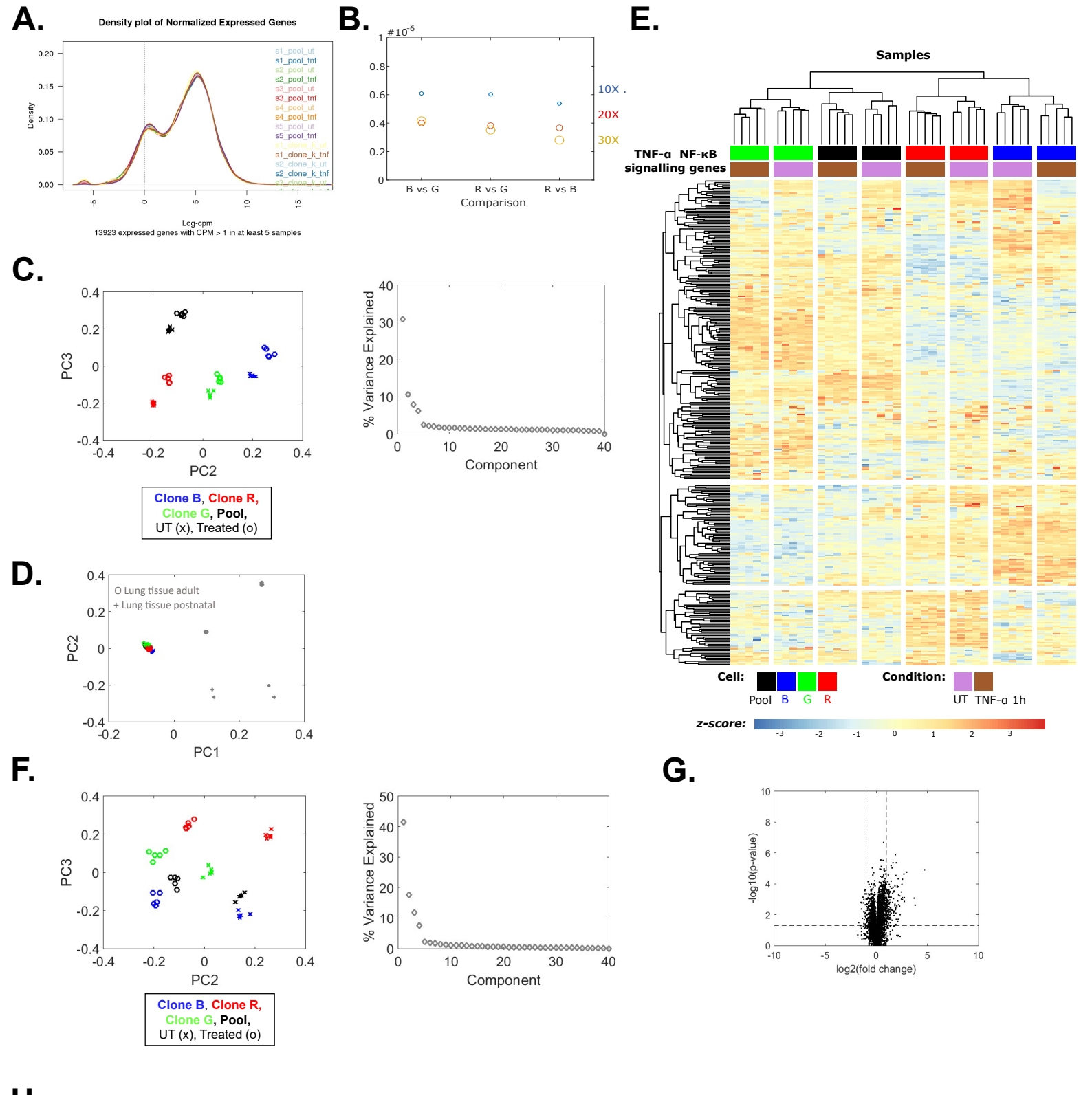

Supp. Figure S4

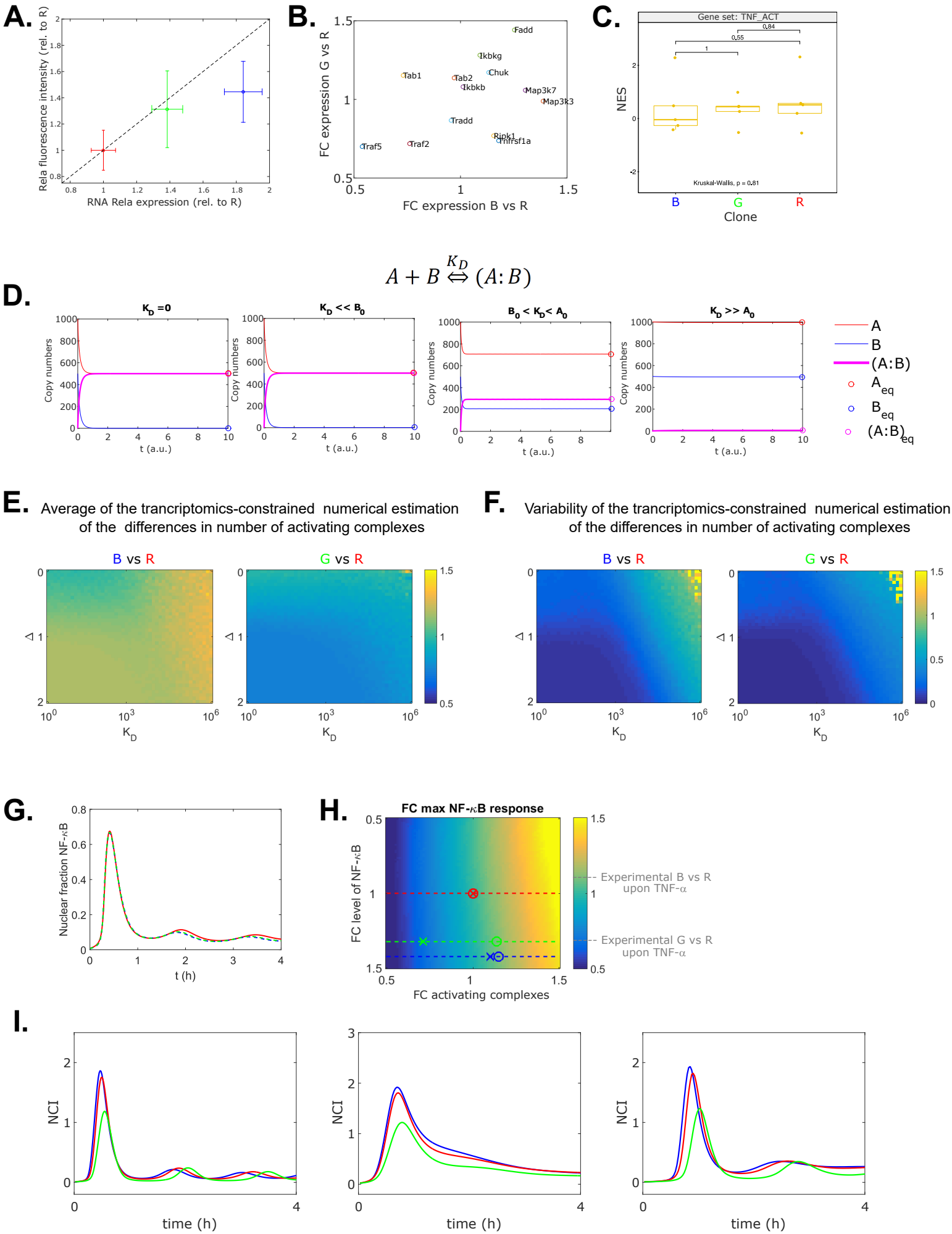

Supp. Figure S5

A.

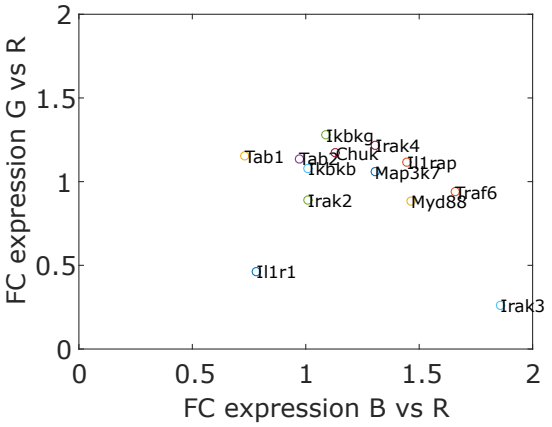

B.

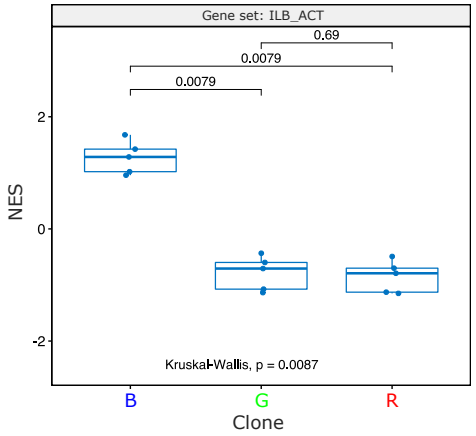

C.

Average trancriptomics-constrained numerical estimation of the differences in number of activating complexes

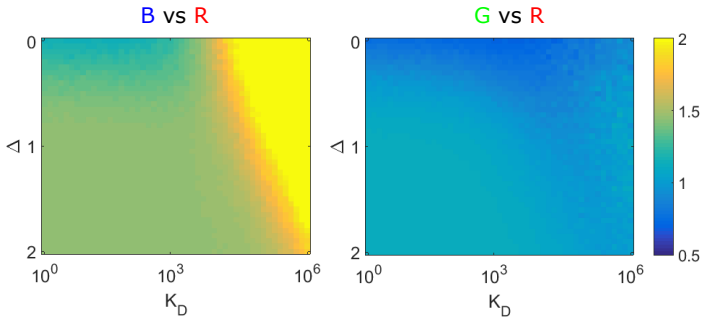

D.

Variability in the Trancriptomics-constrained estimation of the differences in number of activating complexes

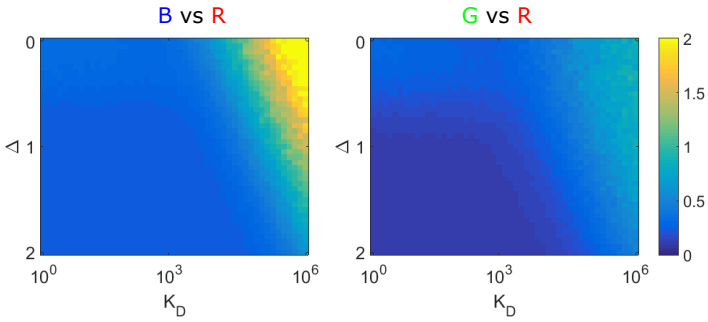

E.

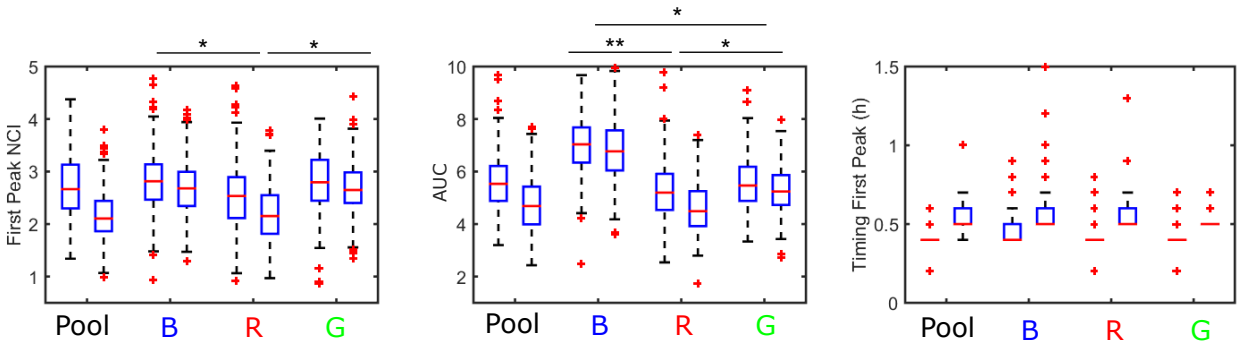

F.

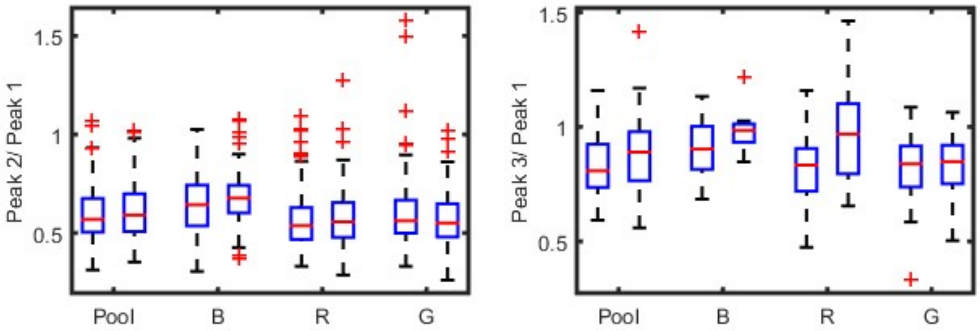
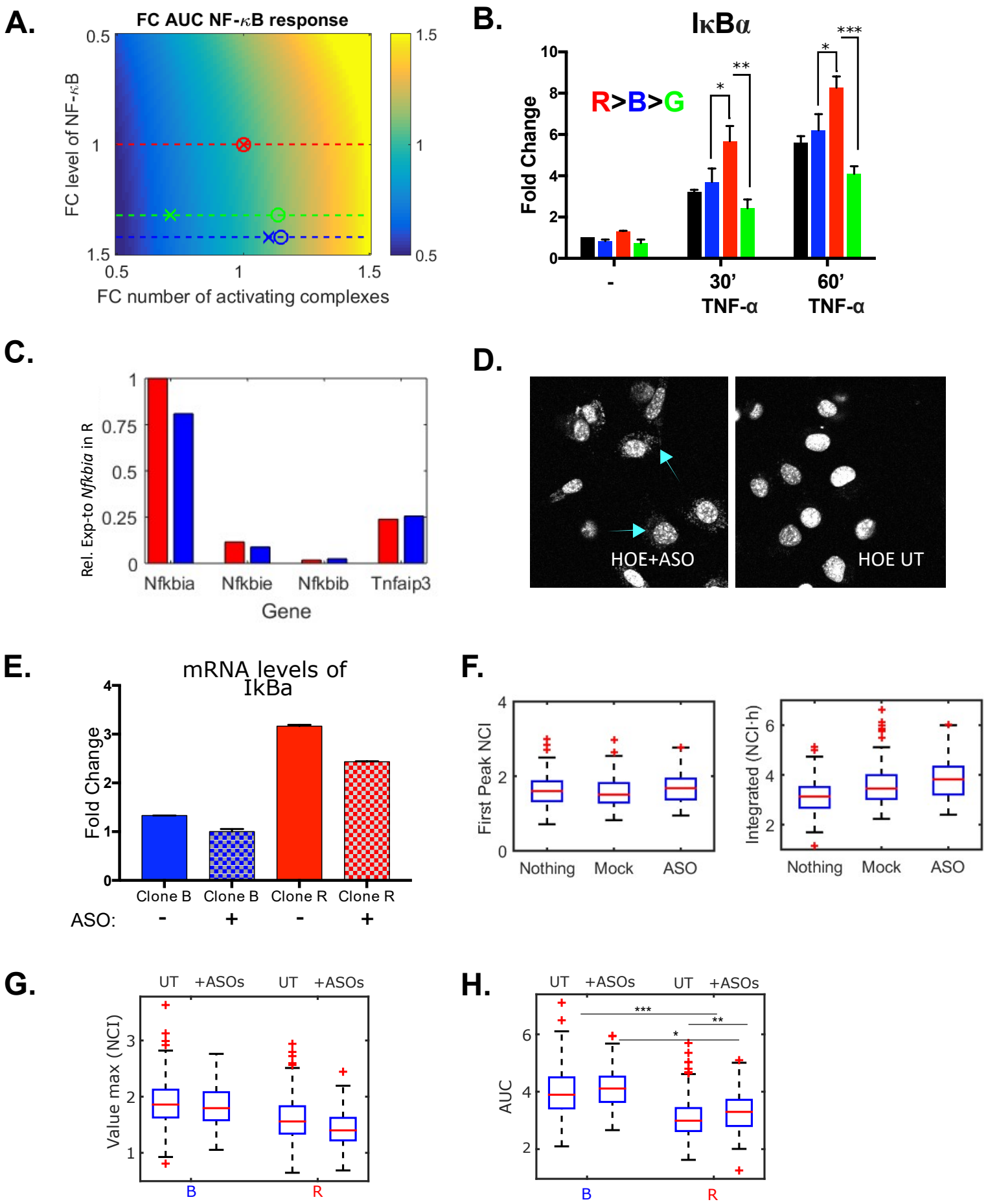
Supp. Figure S6